Investigation into association between cerebral gray matter metrics and cerebrovascular diameters

By

Maryam Alipasandi
A thesis submitted to the Department of
Computer Science in conformity with
the requirements for the degree of
Master of Science

Bishop's University
Canada
August 2022

Abstract

Inter-individual variability in cerebral gray matter metrics including cortical thickness, cortical surface area, and cortical volume have been associated to progression of neurodegenerative disease such as Alzheimer's Disease. However, it is currently unknown what causes these changes in cortical gray matter. One hypothesis is that cerebrovascular degeneration precedes changes in cortical gray matter (reduction in blood supply to the brain results in gradual reduction in gray matter). Brain arterial diameters computed from MRI images can be used to quantify cerebrovascular structure non-invasively in-vivo in humans. However, the relationship between brain arterial diameters and better-known biomarkers such as cortical thickness or surface area is not well understood. To address this, we compared brain arterial diameters in middle cerebral artery and anterior cerebral artery with popular gray matter metrics including cortical thickness and surface area. We find that in general there is an inverse relationship between arterial diameter and gray matter measures, with larger diameters associated to smaller surface area. However, there was a positive correlation between diameters and thickness. We believe that these findings may aid in the understanding of some neurodegenerative diseases such as Alzheimer’s by establishing for the first time a relationship between vascular measures and brain gray matter.

Acknowledgments

I would like to express my deepest gratitude to my supervisor, Dr Russell Butler, for his kind support and providing guidance and feedback throughout this project. Furthermore, I would like to thank computer science chair person, Dr. Layachi Bentabet for his unconditional support. I'm proud of, and grateful for, my time working with his as an international students representer. I am also thankful to the computer science department faculty members and my defense committee for all their thoughtful guidance. Additionally, this endeavor would not have been possible without the support from the Bishop's Graduate Entrance Scholarship Foundation, who financed my research.

Lastly, my family deserves endless gratitude: my parents for teaching me to care about the right things as our lives and resources are finite, my brother for teaching me that an assertion of dominance is not necessarily a bad thing, my sister for teaching me how to have fun and become a laughing person, and my lovely husband for teaching me to live the life as I dream of. To my family, I give everything, including this.

Table of Contents

List of Tables

List of Figures

Chapter 1

Introduction

1.1 Motivation

Alzheimer's disease (AD) is the most common form of dementia and a progressive neurodegenerative disorder [1]. AD risk increases with age, and several pathogens are implicated [2]. However, changes in the brains of people with AD is not known precisely. The most accepted hypothesis is that amyloid-beta deposition causes a cascade leading to neuronal degeneration. Studies revealed a significant reduction of gray matter in the AD group when compared to the healthy group [3]. A number of recent studies have shown that vascular factors also play a role [4]. We reviewed some previous studies that tested the hypothesis that brain arterial dilatation increases the risk of Alzheimer's dementia. They found that the rate ratio of AD was higher among participants with larger normalized brain arterial diameters, indicating that those with larger arteries are at higher risk of AD [5]. With evidence suggesting that vascular risk factors are also associated with AD, the question "Is there any association between arteries and gray matter reduction?" has been posed. Based on these findings, the goal of this study was to understand the association between brain arterial diameter and brain gray matter, which may reveal new clues to the vascular contributions to AD.

1.2 Objective

The aim of this study was to investigate the relationship between the cerebral arterial diameter and cortical gray matter metrics (thickness, curvature, and surface area), advancing our understanding areas of the brain affected by vascular diseases.

1.3 Summary

In this study, we present a review of the fundamentals of Magnetic Resonance Imaging (MRI) and brain anatomy. Then, we cover some previous studies related to arterial diameter from Time Of Flight (TOF) images and morphometry analysis. In chapter 3, we provided an image processing pipeline to isolate, extract, and quantify cerebral vessels in TOF angiography. We apply two different approaches, 1) voxel-based morphometry analysis and 2) region-based analysis, resulting in correlation maps for associating arterial diameter to brain metrics. We find

that in general there is an inverse relationship between arterial diameter and gray matter measures, with larger diameters associated to smaller surface area. However, there was a positive correlation between diameters and thickness.

Chapter 2

Literature Review

Fundamentals of Magnetic Resonance Imaging (MRI) and brain anatomy are discussed in this chapter, followed by a review of previous studies on artery diameter from TOF images and morphometry analysis.

2.1 Brain anatomy and cerebrovascular system

Although the brain is an immensely complex structure, its anatomical structure can be broken up into more discrete portions; left and right hemispheres, parietal, temporal, occipital, and frontal lobes. The brain can also be divided according to tissue type (gray and white matter). Gray matter, named for its pinkish-gray color, is home to neural cell bodies, axon terminals, and dendrites, as well as all nerve synapses. At the same time, the white matter of the brain and spinal cord is composed of bundles of axons. Cerebral vasculature structures possess highly specialized functions that assure constant brain perfusion, which is necessary for nerve cells and glial cells to obtain the oxygen and glucose they need. There are two components of cerebrovascular anatomy, either endocranial or exocranial, which can be further subdivided into anterior or posterior circulation based on the contribution of cerebral arteries and vertebral arteries, respectively [6]. The anterior circulation of the cerebrum consists primarily of the anterior and middle cerebral arteries. In this study, we intend to extract the diameter of these arteries.

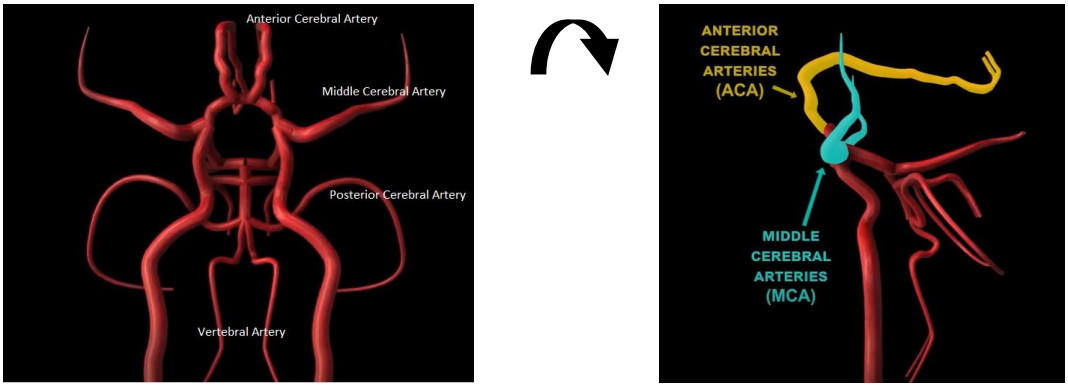

Figure 1. Anterior and middle cerebral arteries in cerebrovascular anatomy

Anterior cerebral arteries arch back along the sagittal plane and supply the middle aspect of the cerebral hemispheres back to the parietal lobes and medial rostral portion of the hemisphere. Middle cerebral arteries run along the lateral sulcus, branching off and supplying a large portion of the cerebral cortex and lateral rostral. The posterior cerebral arteries go around the cerebral peduncles, run over the top of the tentorium cerebellum and supply the posterior medial surface of the temporal and occipital lobes and medial caudal portion of the cerebrum [7].

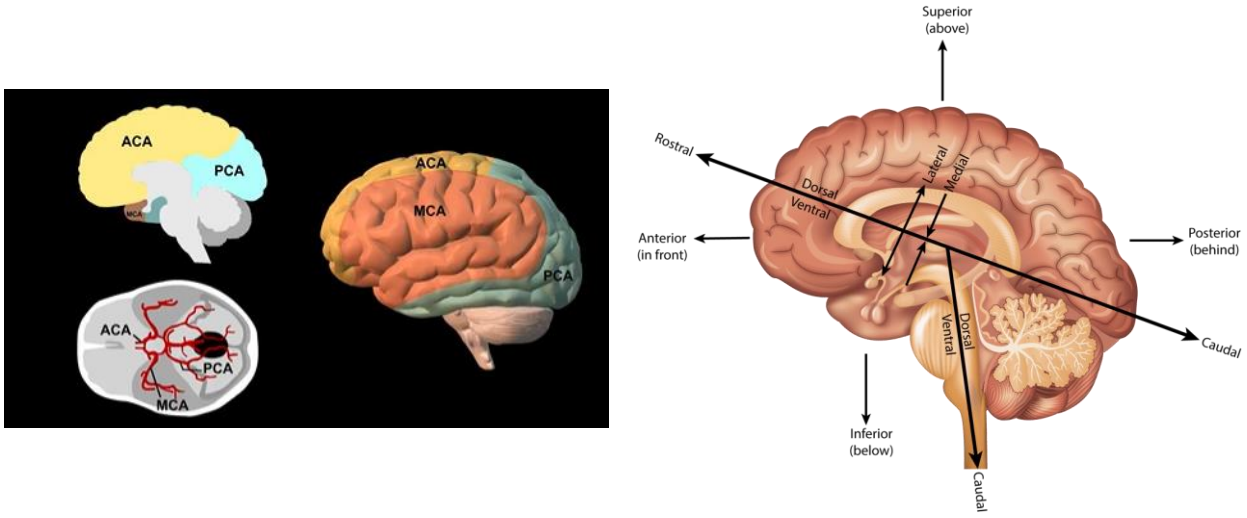

Figure 2. A diagram to summarize the cortical vascular territories [8]

2.2 Magnetic Resonance Imaging

MRI is a medical imaging technique mainly used in radiology and nuclear medicine for investigating anatomy and physiology, and detecting problems with muscles and joints, along with abnormalities related to the heart and blood vessels. Magnetic fields produced by an MR system mainly result from large currents flowing through a loop of wires connected to the magnet of the imaging system. Protons in the body, which are positively charged and spin about their axes, act as tiny magnets. They are oriented in such a way that their magnetic fields cancel one another rather than summing [9].

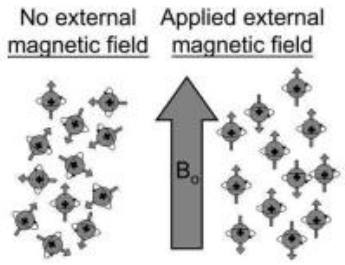

Figure 3. Alignment of protons with/without the magnetic field [9]

When we place these protons in a strong magnetic field (called B0), some will tend to align in the direction of the magnetic field, and some will tend to align in a direction opposite to the magnetic field. The magnetic fields from many protons will cancel out. Still, a slight excess of the protons will be aligned with the main magnetic field, producing a "net magnetization" that is aligned parallel to the main magnetic field. This net magnetization becomes the source of our MR signal and is used to produce MR images [9]. The proton processional frequency is determined from the Larmor equation, in which the frequency of precession, f, is equal to a constant (γ) times the main magnetic field strength (B_0). The γ is called the gyromagnetic ratio and is a characteristic of each type of nuclei. For hydrogen, the gyromagnetic ratio is 42.58 MHz/Tesla, which yields a Larmor frequency of 127.74 MHz for hydrogen at 3 Tesla. We call this the resonant frequency of hydrogen at 3 Tesla. A spinning proton (hydrogen atom) is a moving charge, which creates a measurable magnetic field [10].

$$f = \gamma B_0 \qquad \text{Larmor Equation}$$

As energy is absorbed from the Radio Frequency (RF) pulse, the net magnetization rotates away from the longitudinal direction. The strength and/or duration of the RF pulse can be controlled to rotate the net magnetization to any angle. After a 90° RF pulse, protons that were in phase begin to dephase in the transverse plane due to effects discussed earlier (represented by some spins going faster than the average and some spins going slower than the average). After a certain amount of time, if a 180° RF pulse is applied, the spins will rotate over to the opposite axis. Now, rather than the spins continuing to dephase, the spins will begin to rephase. The rephasing of the spins forms an "echo" called a spin echo. The time between the peak of the 90° RF pulse and the peak of the echo is called the time to echo or echo time (TE). TR is the time that it takes to run through the pulse sequence one time [11].

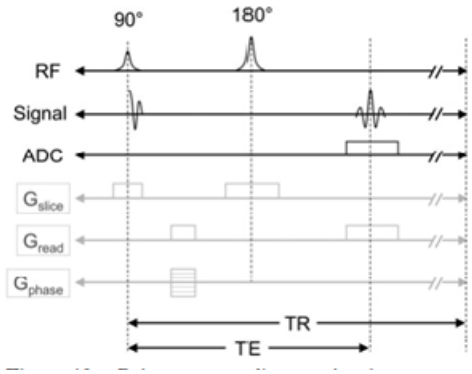

Figure 4. Pulse sequence diagram [11]

Magnetic resonance imaging (MRI) is an extremely flexible imaging technique that can capture a wide range of soft tissue contrasts. Differences in contrast, field of view, and spatial resolution exist between T1-weighted and TOF MRI. T1-weighted images and T2-weighted images capture the contrast between gray matter and white matter. However, Time-of-flight images (TOF) capture contrast between arteries and surrounding tissue. In TOF MRI, the field of view is smaller, but the spatial resolution is higher.

T1-weighted images T2-weighted images Time-of-flight images (TOF)

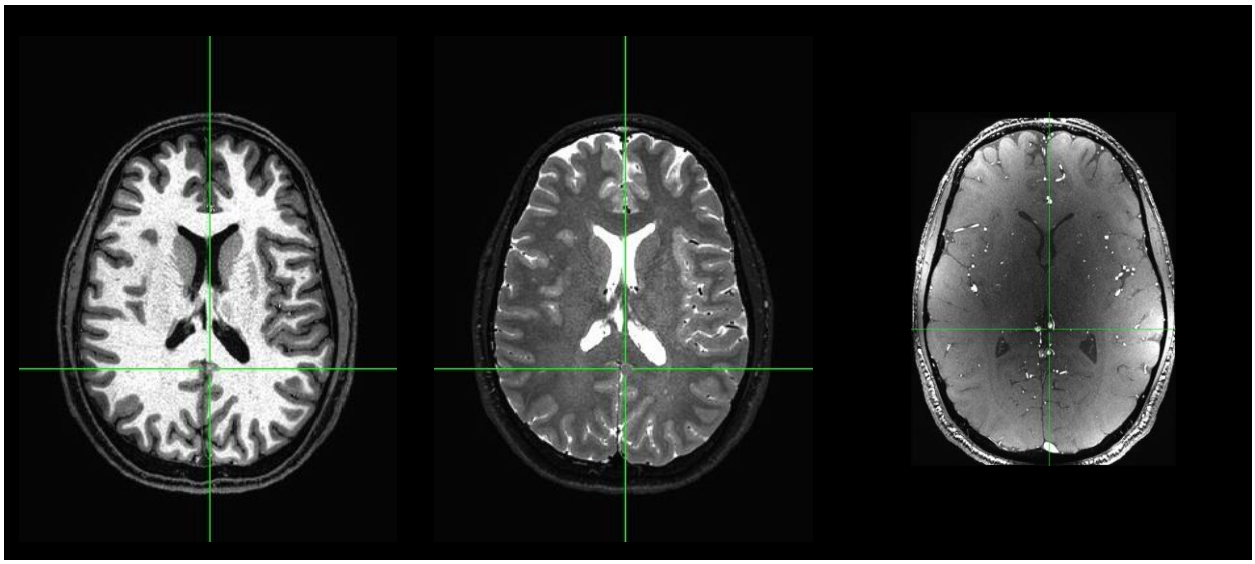

Figure 5. Different MRI modalities for same subject

2.2.1 T1-weighted image

T1 is the time it takes for the longitudinal magnetization to reach 63% of its final value using a 90° RF pulse. For white matter, the T1 time is very short, and it relaxes very quickly. Cerebrospinal Fluid (CSF) has a long T1 and slowly relaxes. In gray matter, T1 is intermediate, and relaxation is intermediate. Image contrast between the tissues is maximized if we acquire the signal at a time when the curves are maximally separated. White matter makes the lighter pixels, CSF makes the darker pixels, and gray matter makes the pixels with intermediate shades of gray [12].

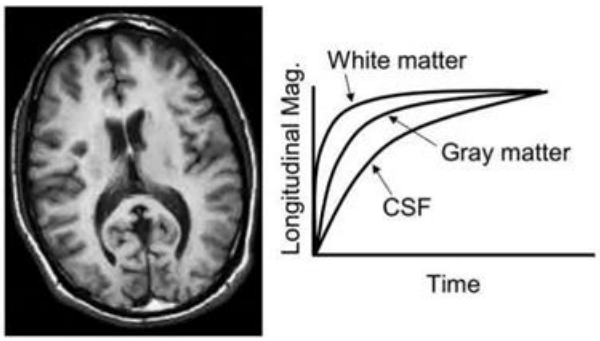

Figure 6. Different tissues with different rates of T1 relaxation [12]

2.2.2 T2-weighted image

T2 is the time it takes for the transverse magnetization to decay to 37% of its original value. Different tissues have different values of T2 and dephase at different rates. White matter has a short T2 and dephases rapidly. CSF has a long T2 and dephases slowly. The gyromagnetic ratio is a constant; however, owing to hardware limitations, the main magnetic field is not perfectly homogeneous across the imaging volume. Thus, protons that experience slightly different magnetic field strengths will process at slightly different Larmor frequencies [12].

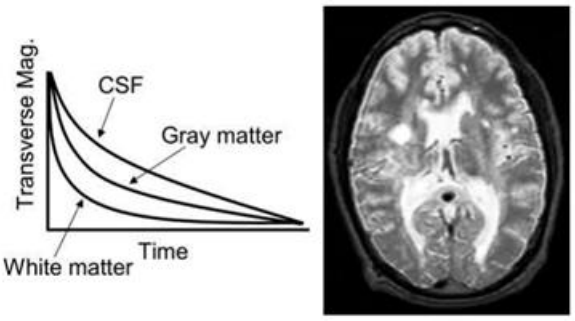

Figure 7. Different tissues with different rates of T2 relaxation [12]

2.2.3 TOF

The Time-Of-Flight (TOF) effect occurs as a result of blood flow between pulses of RF energy. Time of flight (TOF) effects depends on the displacement of blood with respect to a region of excitation. TOF (or wash-in/wash-out) effects are used to study flow in a small segment of the blood vessel. Vessel conspicuity is greatly enhanced by suppressing static material signals which would otherwise dominate. The static material component in the measurement is minimized by reducing its steady-state amplitude through excitation and timing parameters [13].

All blood within the imaging slice of thickness Δz will experience the 90° excitation pulse in a spin-echo sequence. During the time between the 90° excitation pulse and the 180° refocusing pulse (TE/2), the excited blood will have flowed, either partially or entirely, out of the slice and fresh, i.e., unexcited, blood will flow into the slice. If the blood completely washes out of the slice between the two pulses, then the lumen appears dark or hypointense. On the other hand, a bright signal is possible in extremely slow flow due to the wash-in of unsaturated spins with a large longitudinal magnetization between TRs, along with a lack of wash-out. An example of the TOF effect in spin-echo imaging is shown in Figure 8 [14].

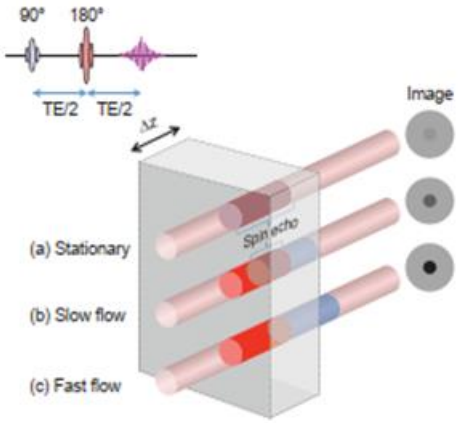

Figure 8. Effect of time of flight in spin-echo imaging [14]

TOF effects in gradient-echo imaging generally appear as a signal hyperintensity due to the in-flow of fresh blood that has not experienced any prior RF pulses into the imaging slice between TRs. The degree of enhancement will depend upon the velocity (v), slice thickness (Δz), and TR. As long as v equals or exceeds Δz /TR, during TR the blood is replaced with fresh, unsaturated blood, resulting in the maximum signal. When v is less than Δz/TR there is an only partial replacement of spins resulting in reduced signal intensity [14].

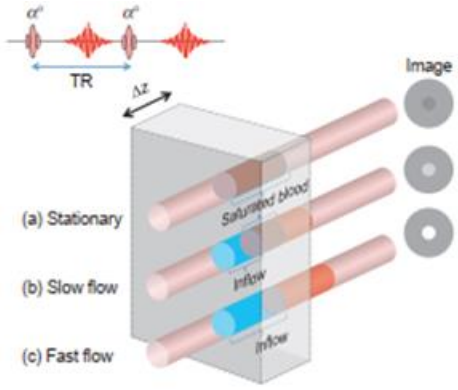

Figure 9. Effect of time of flight in gradient-echo imaging [14]

2.3 Studies of arteries diameter from TOF images

Using susceptibility weighting imaging (SWI) and time-of-flight angiography (TOF-MRA), [15] designed a fast, open-source algorithm using advanced vessel segmentation schemes and iterative nonlinear registration to isolate, extract, and quantify cerebral vessels. The results show that regional variations in both venous and arterial density were significantly correlated to

cortical thickness. In spite of the availability of numerous neuroimaging tools for segmenting and quantifying gray and white matter, relatively few non-invasive public methods exist for investigating cerebral blood vessels. By comparing the vascular tree between healthy controls and patient populations in an automated way, researchers in [16] quantified normal variations in vessel density and diameter. TOF and SWI permit visualization of the large arteries and veins, respectively, on a single-subject basis [17]. An automatic method for reconstructing cerebral arterial vessels and determining their diameter on a voxel-by-voxel basis was developed by [18]. The researchers measured the vasodilation induced by visual stimulation in the posterior cerebral artery (PCA) supplying each occipital lobe. They used Euclidean distance transform to estimate diameter and unsampled the data to 0.1*0.1*0.1 mm resolution to improve the measurement accuracy.

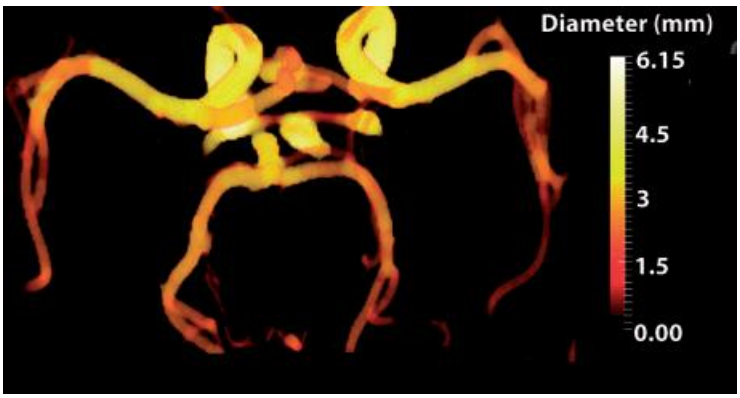

Figure 10. Posterior artery segmentation is color-coded as a function of diameter [18]

Another study [19] compared diameters extracted from TOF with transcranial doppler sonography

in the middle cerebral artery, hoping to demonstrate a lack of diameter change in the insonated vessels during a hyperventilation task. They used 0.8*0.4 mm in-plane resolution to study the intracranial vessels, showing no significant deviation of vessel diameter during the task.

In general, TOF is accepted as a technique for follow-up imaging on aneurysm patients, and recent work shows deep learning algorithm detected intracranial aneurysms with high diagnostic performance in a retrospective study [20] on a training set of 468 images and a test set of 120 images.

2.4 Morphometry analysis

Human brain volume and structure are affected by several factors. A decrease in brain volume and an increase in cerebrospinal fluid (CSF) space have been observed with aging through magnetic resonance imaging (MRI) and computed tomography [21, 22]. The atrophy of the medial temporal lobe is one of the earliest symptoms of AD, accompanied by hippocampal atrophy, the most visible pathological symptom [23]. Morphometry analysis can demonstrate these changes clearly and are key to constructing diagnostic models [24]. Several investigations have been conducted on gray matter volume changes with advancing age. In a Voxel-Based Morphometry (VBM) analysis [25], most cortical regions, predominantly in the frontal and insular areas, have shown a linear negative association between volume and age.

On the other hand, [26] has found the preservation of gray matter volume in specific structures such as the Amygdala, Hippocampus, and Thalamus. In a recent study [27], two experimenters, under the guidance of radiologists, manually divided the regions of interest, namely the hippocampus, using a region growing approach. They built various Elaboration Likelihood Models (ELM) according to different characteristic variables. They showed that the effect of modeling with only VBM parameters was better than that of modeling with only texture parameters. The VBM parameters belong to the three-dimensional parameters, while texture features belong to the two-dimensional plane parameters. VBM parameters can describe and distinguish the macroscopic and neuroanatomical differences between different brain regions and clearly identify gray matter differences between subjects.

Surface-based morphometry tools have made it possible to quantify gray matter in the human brain in a more automated fashion [28]. Software packages such as FreeSurfer provide measurements of cortical and subcortical gray matter features based on MRI data. This surface-based morphometry can measure not only volume but also cortical thickness. Using this technique, [29] computed the association of cerebral cortical thickness with memory performance and depressive state in participants with mild cognitive impairment (MCI).

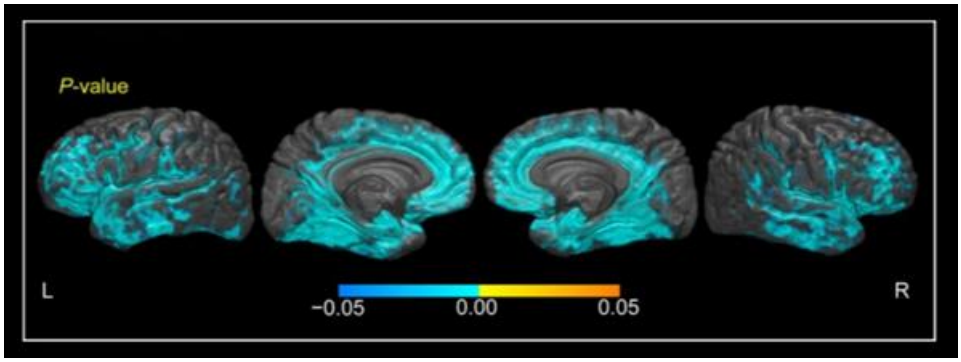

Figure 11. Association of cerebral cortical thickness and WMH volume [29]

How gray matter changes in normal aging is investigated in [30]. VBM and voxel-based cortical thickness measures yield overall consistent results when investigating healthy aging, but voxel-based cortical thickness provides a more sensitive measure of the age-associated decline in gray matter compared with VBM.

Chapter 3

Materials and Methods

3.1 Dataset and environment

3.1.1 AFNI

AFNI (Analysis of Functional NeuroImages) is a leading software suite of C, Python, R programs, and shell scripts primarily developed for the analysis and display of multiple MRI modalities: anatomical, functional MRI (fMRI), and diffusion-weighted (DW) data. It is freely available for research purposes (both open-source code and precompiled binaries). AFNI can be easily used on Linux/Unix and Mac systems [31].

3.1.2 OpenNeuro

OpenNeuro is a new platform providing easy access to high-resolution, state-of-the-art datasets. It is organized with reproducibility in mind and provides new incentives for neuroscientists to share their data. Data files are organized according to the standards implemented by the openfmri.org project [32].

We used the Forrest dataset from OpenNeuro, a collection of brain images of both T1-weighted and TOF (7-Tesla) from 20 different people. Additional material is available at http://www.studyforrest.org. This includes information on data access options and publications that employ this dataset, as well as source code for data conversion and the processing steps.

3.1.3 Participants

Twenty right-handed volunteers (age 21-38 years, mean age = 26.6 years, 12 male) native language of all participants was German. All reported normal hearing with no impairments or history of neurological disorders. In each completed MRI session, T1 and TOF were acquired with a Siemens MR scanner at 7-Tesla using a 3D multi-slab sequence (0.3 mm isotropic voxel size) at 7 Tesla. Participants were instructed to inhibit any physical movements within the scanner and were asked to move as little as possible. Subjects listened to background music throughout the scans.

3.2 Arteries Diameter extraction

Following is a flowchart that shows how we extract arteries' diameter step by step.

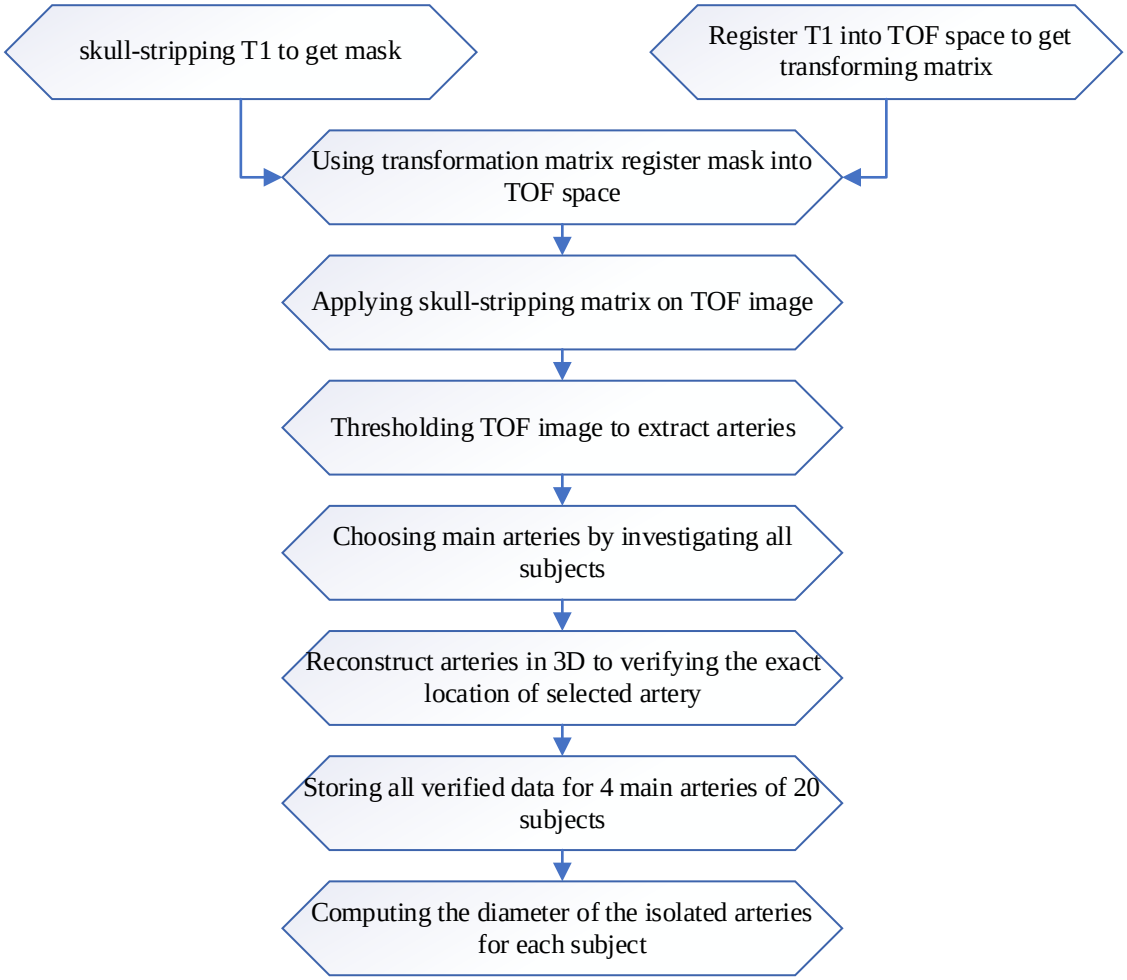

Since this study focus on brain tissue, our first step is to remove the skull and non-brain areas from the image. FSL has a tool called bet, or the Brain Extraction Tool. It is a very robust and automated method for segmenting magnetic resonance head images into brain and nonbrain parts. It has been tested on thousands of data sets from a wide variety of scanners and taken with a wide variety of MR sequences [33].

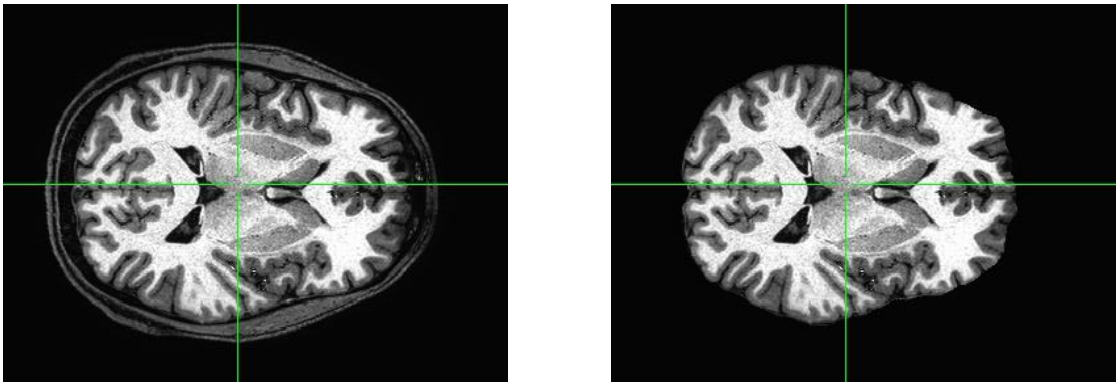

Figure 12. Extracted brain from T1-weighted image

As bet can be used on T1 and T2 input images, we saved the mask for extracting the brain area. Then, to remove the non-brain area from the TOF image, we register the bet mask on the TOF space. Image registration aims to find the best spatial alignment between two or more images of the same scene, which have been taken at different times or with the same/different devices in a single/multi-view fashion [34].

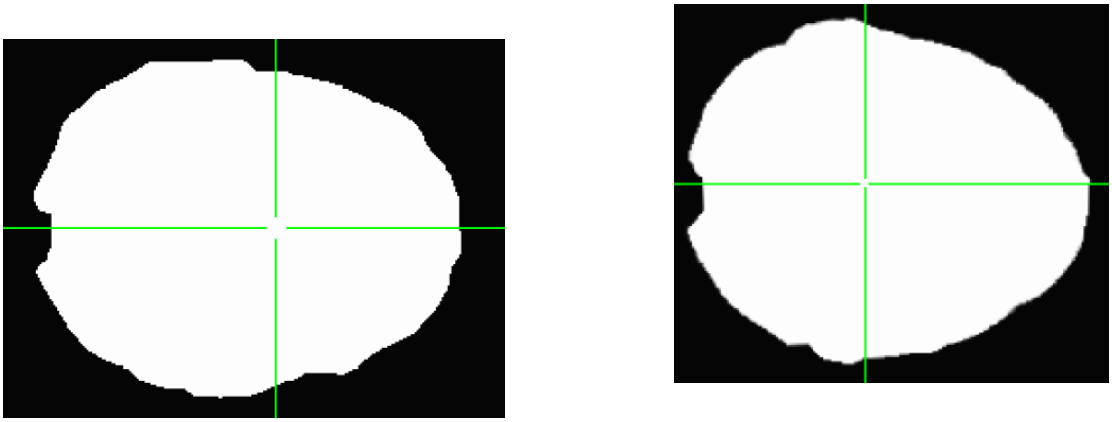

Figure 13. Non-brain area remover mask transformed from T1 space to TOF space

Applying a skull-stripping mask on TOF images, we have the non-brain area removed and ready to extract arteries.

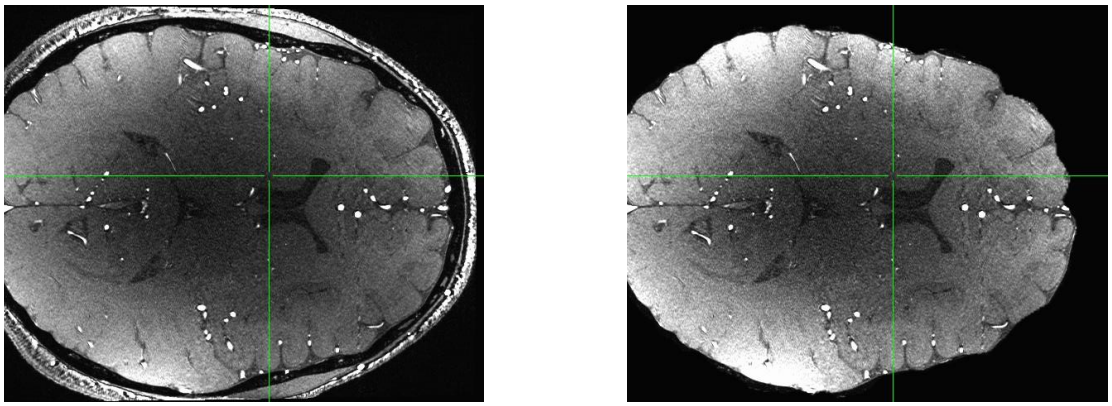

Figure 14. Extracted brain from TOF image

Skull-stripped TOF image is preprocessed and ready to extract arteries using a thresholding method. Thresholding is an often-used tool in the segmentation of medical images. Segmentation s of an image f by threshold t at voxel $\boldsymbol{v}$ is given by:

$$s(\boldsymbol{v})=\begin{cases}1 & if\ f(v) > t \\ 0 & otherwise\end{cases}$$

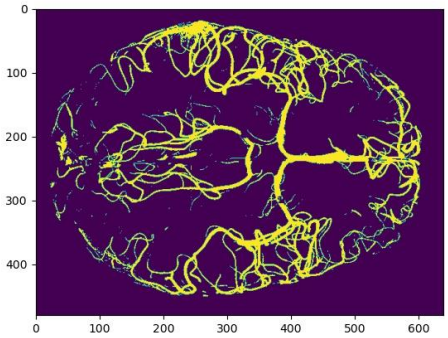

Figure 15. Extracted arteries by thresholding TOF image

Several different arteries can be used for diameter data collection. Investigating all participants' MRI images, we came to this conclusion that our choice is the middle cerebral artery and anterior cerebral artery. The main factor in selecting arteries was their detectability in all subjects MRI images. For example, as the field of view in TOF MRI is limited, the posterior cerebral artery is not shown in some cases.

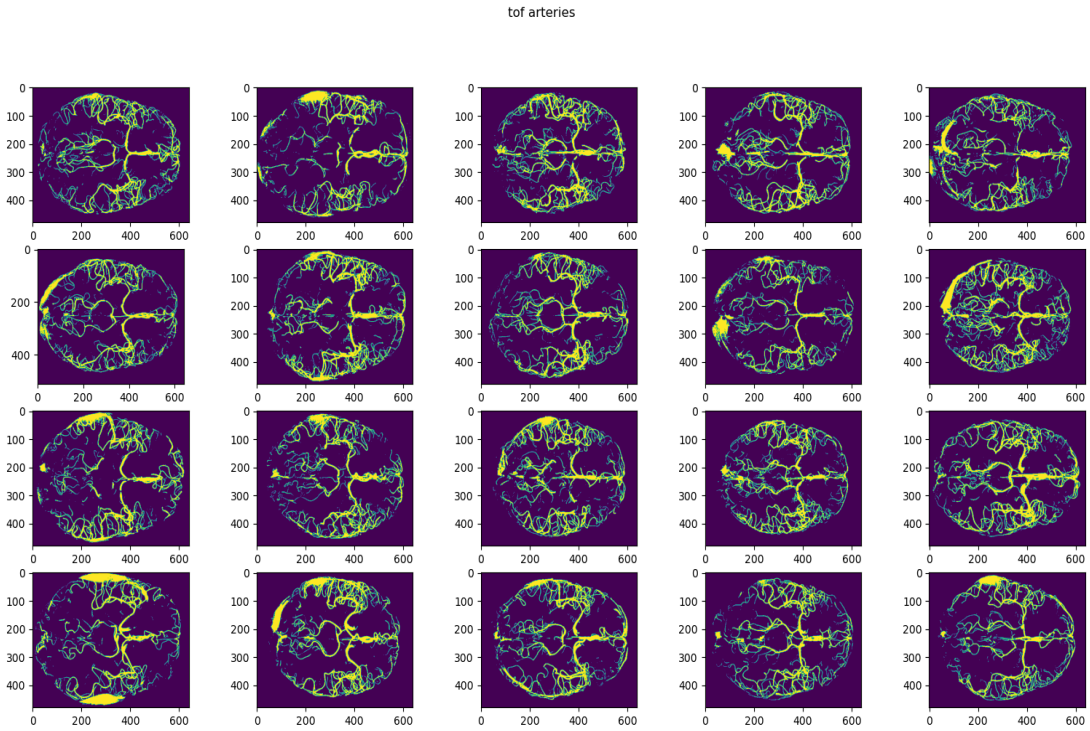

Figure 16. All participants extracted arteries

To find the exact location of chosen arteries, by determining points on x-axis and z-axis first, and then pinpointing the third coordinate on the y-axis. Then, to verify the exact location of the chosen point of each artery reconstructing cerebral arteries in fiber navigator, we visualized all points in 3D.

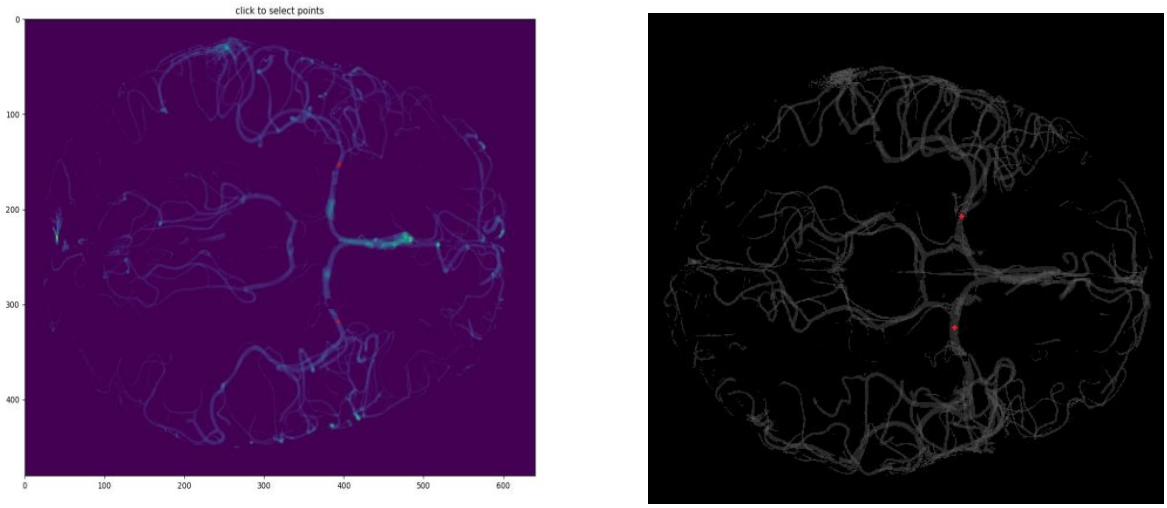

Figure 17. Pinpointing middle cerebral artery (MCA) in 2D and 3D

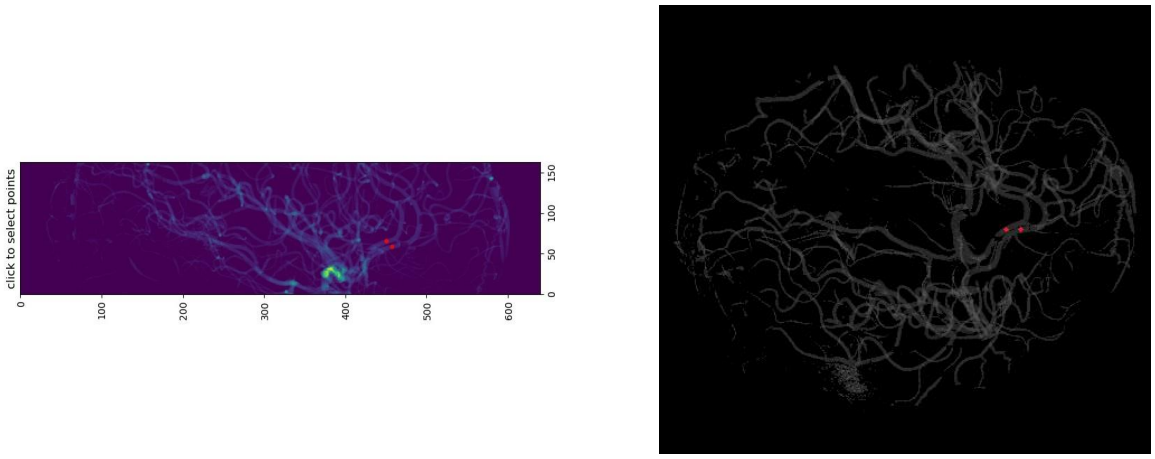

Figure 18. Pinpointing anterior cerebral artery (ACA) in 2D and 3D

Diameter extraction was done by labeling a slice of images based on the arteries coordination and finding the exact labeled diameter. The labeling algorithm uses a scanning step that examines some of its neighbors and the connectivity. Two pixels are connected when they are neighbors and have the same value. In 2D, they can be neighbors either in a 1- or 2-connected sense. The value refers to the maximum number of orthogonal hops to consider a pixel/voxel a neighbor. We used 8-connected components in a 2D image.

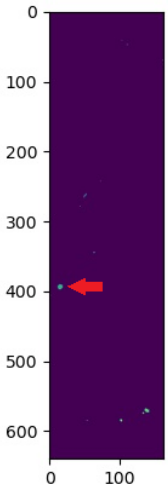

Figure 19. Labeled **e**xtracted arteries diameter

3.3 Morphometry Analysis

The morphometry analysis of the brain refers to the measurement of the size, volume, and shape characteristics of different brain structures and tissue types, which has been done using two different approaches:

a) Voxel-based morphometry
b) Region-based morphometry (FreeSurfer measurements)

Each approach is accompanied by a correlation brain map.

3.3.1 Voxel-based morphometry

Voxel-based morphometry (VBM) is a neuroimaging technique investigating focal differences in brain anatomy. The objective of VBM is to localize regions (in stereotaxic space) where there are significant differences. The core process of VBM is segmenting the brain into grey matter, white matter, and cerebrospinal fluid, warping the segmented images to a template space and smoothing. After that, statistical analysis is performed.

3.3.1.1 Segmentation

An approach to a three-compartment segmentation is multi-channel tissue segmentation. Using the FSL tool and FAST command, T1 was used to estimate gray matter, white matter, and CSF compartments.

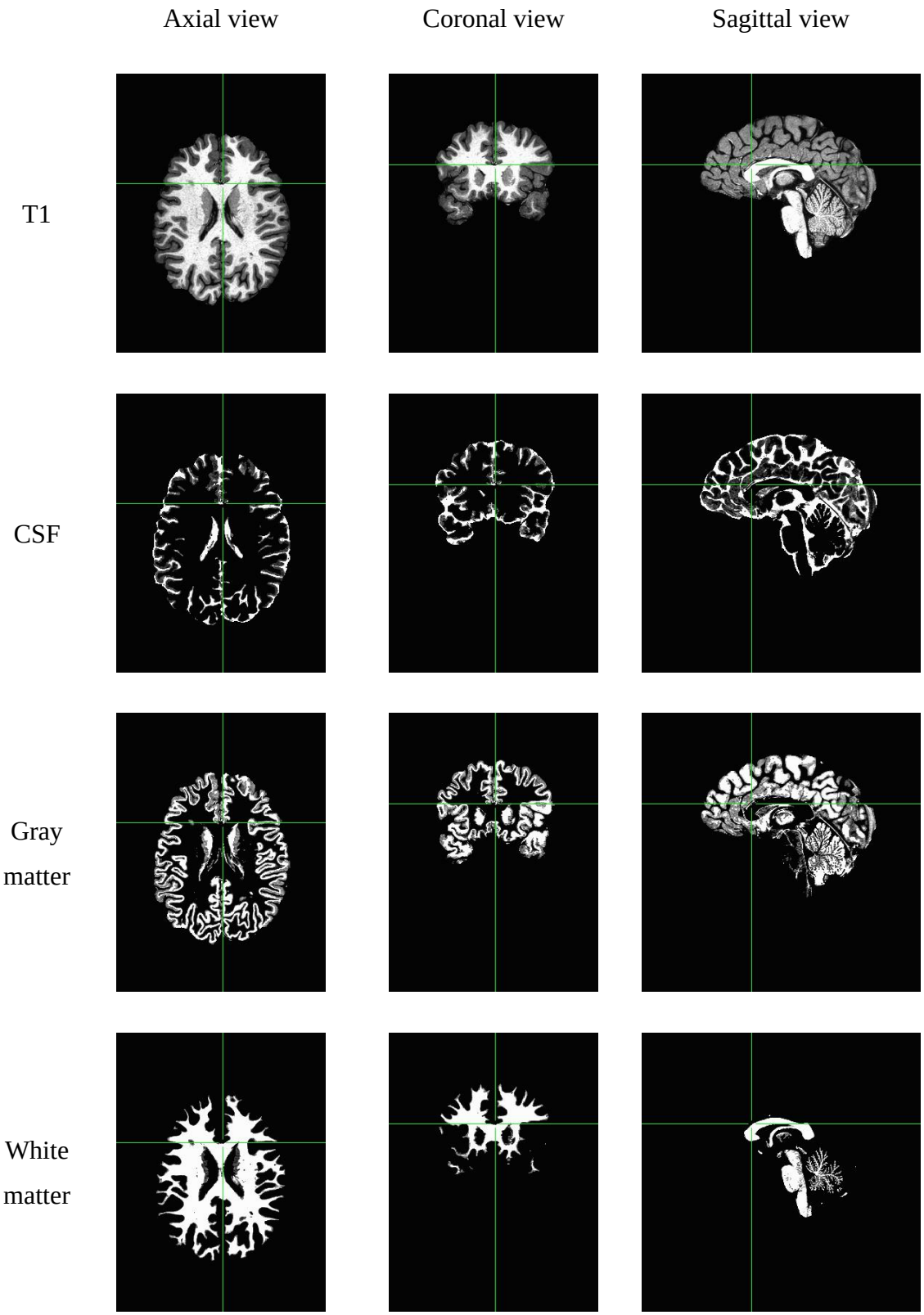

Figure 20. Gray matter, white matter, and CSF segmented from T1 weighted image

3.3.1.2 Spatial normalization

Spatial normalization involves warping all the gray matter images to the same space, which is achieved by matching to a standard template image. MNI (Montreal Neurological Institute) was used as our template brain. The MNI defined a standard brain by using a large series of MRI scans on normal controls. There are many registration methods that can be used for this. FLIRT (FMRIB's Linear Image Registration Tool) is a fully automated, robust, and accurate tool for (affine) intra- and inter-modal brain image registration. It tries to find the transformation that best aligns the images, using a customized global optimization technique that operates over multiple resolutions. Once the best transformation has been found, the original input image is resampled and transformed to match the reference image. The final output image will contain intensities derived from the input image but will have a field of view and voxel size that matches the reference image. When the images are of different subjects, in this case registering to standard space, 12 DOF is appropriate for large FOV.

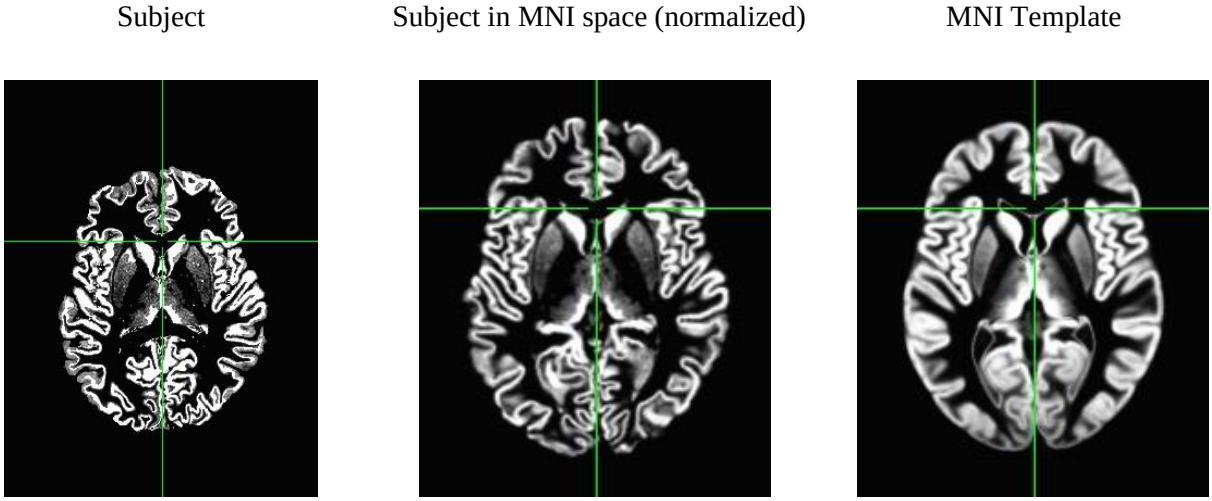

Figure 21. Normalizing gray matter of each subject

3.3.1.3 Smoothing

Image registration results in some regions growing and others shrinking. Thus, we smoothed the warped gray matter images by convolving them with an isotropic Gaussian kernel. This makes the subsequent voxel-by-voxel analysis comparable to a region of interest approach because each voxel in the smoothed images contains the average amount of gray matter from around the voxel. Smoothing also has the effect of rendering the data more normally distributed, thus increasing

the validity of parametric statistical tests. The smoothing kernel was Gaussian with a full width at half maximum (FWHM) of 10 mm.

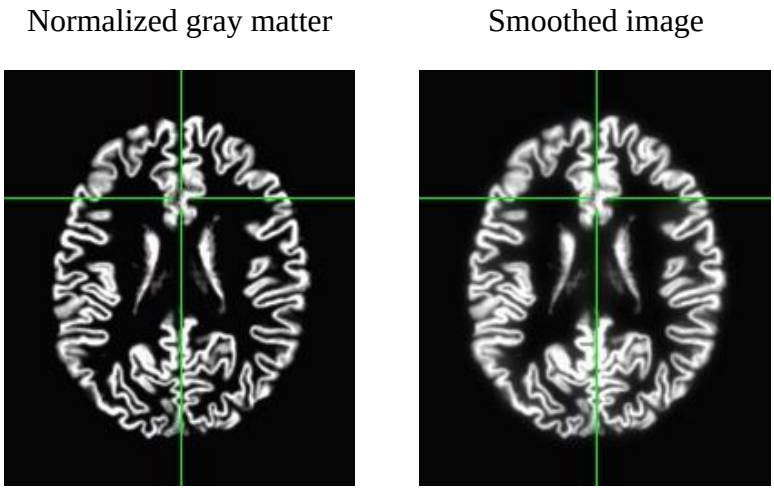

Figure 22. Smoothing normalized image

3.3.2 FreeSurfer

FreeSurfer is a software package for the analysis and visualization of structural and functional neuroimaging data from cross-sectional or longitudinal studies. FreeSurfer extracts a cortical surface and calculates structural measurements at each vertex. In the cortical surface stream, the tools models the boundary between white matter and cortical gray matter as well as the pial surface [35]. Once these surfaces are known, an array of anatomical measures becomes possible, including cortical thickness, surface area, curvature, and surface normal at each point on the cortex. We used FreeSurfer to compute four features (area, thickness, mean curve, volume) for each cortical region of the subjects.

Chapter 4

Results and Discussion

4.1 Arteries diameter correlation

We compared the left and right sides of both types of arteries diameter by extracting the diameter of all subjects' arteries. While different types of arteries did not show a meaningful association, the same type of artery diameters correlated significantly.

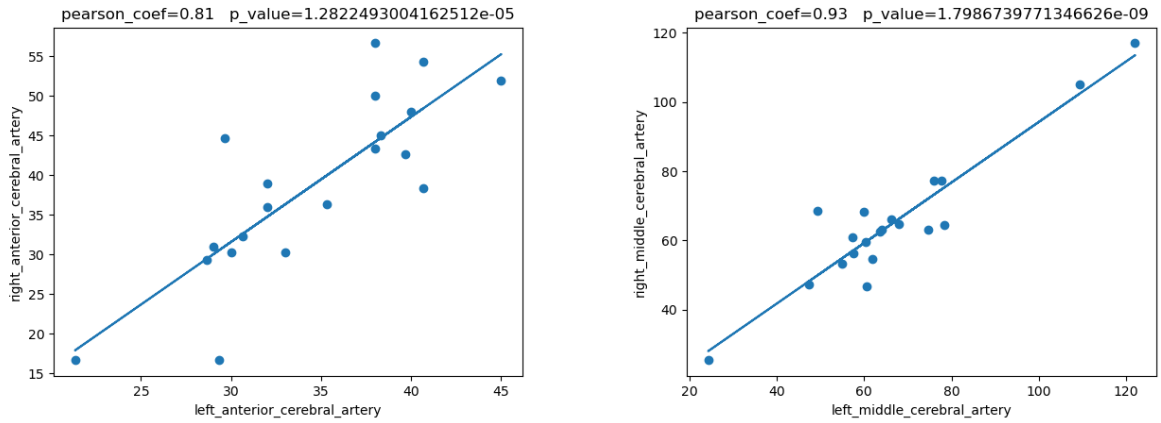

Figure 23. Same arteries diameter has a significant correlation in two side

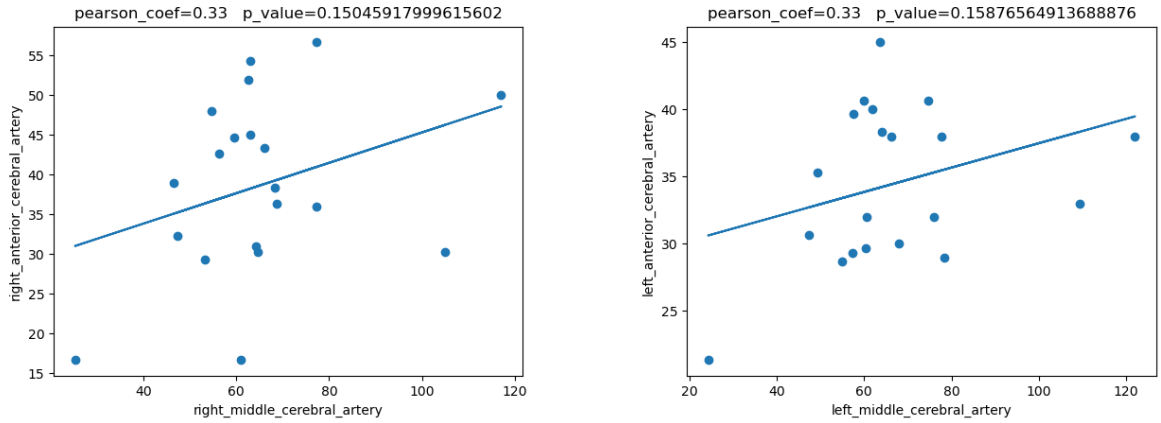

Figure 24. Different arteries diameter has insignificant correlation even on the same side

4.2 Correlation maps

4.2.1 Voxel-based correlation between gray matter and arteries diameter

We generated the voxel-based correlation maps between the smoothed normalized gray matter produced in the 3.3.1 sector and each artery's diameter defined in the 3.2 sector (left & right middle and anterior cerebral arteries). As we did not expect a linear relationship, the Spearman correlation coefficient which is widely regarded as a nonparametric technique, is used in this study.

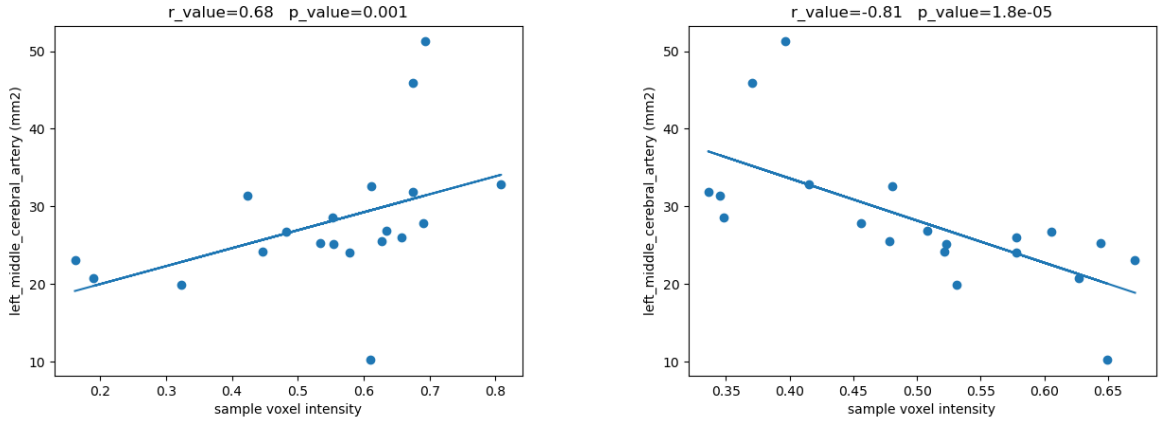

Figure 25. correlation between two sample voxels intensity and left MCA's diameter

Correlation maps are the correlation values (r-value) projected onto the single standard subject (MNI brain template) for display purposes. In these maps, color clustering is based on r-value ranging from -1 to 1 in 6 classes. For positive correlation, it varies from yellow to red, and for negative ones, we used light to dark blue.

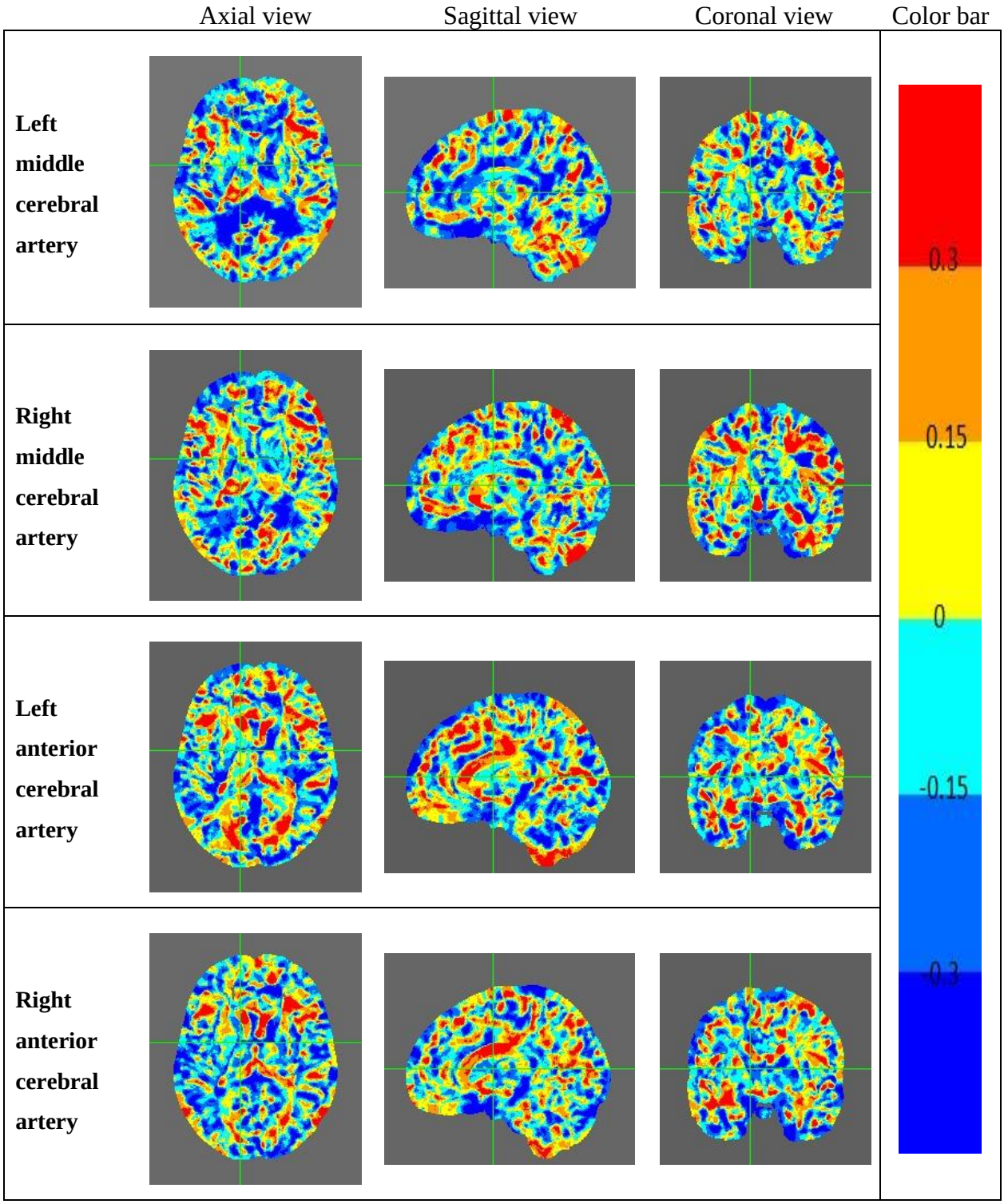

Figure 26. Correlation maps between gray matter and arteries diameter

The mean correlation for each artery is shown in Table 1. We offered mean values separately for directly correlated and adversely correlated data since correlations are either negative or positive.

Table 1. Mean correlation value of gray matter with each arteries diameter

	Left middle cerebral artery	Right middle cerebral artery	Left anterior cerebral artery	Right anterior cerebral artery
Positive values mean	0.17	0.17	0.18	0.17
Negative values mean	-0.2	-0.19	-0.20	-0.19
Total mean	-0.04	-0.02	-0.03	-0.03

Suppose we plot the voxels portion with a negative or positive correlation to arteries diameter. In that case, the results show that the negatively correlated share of gray matter is much more than positively correlated to the diameter of arteries. However, the last row of Table 1 shows that the mean correlation value of gray matter with each artery's diameter is around 0, which means there is no general correlation between gray matter and arteries diameter using VB approach.

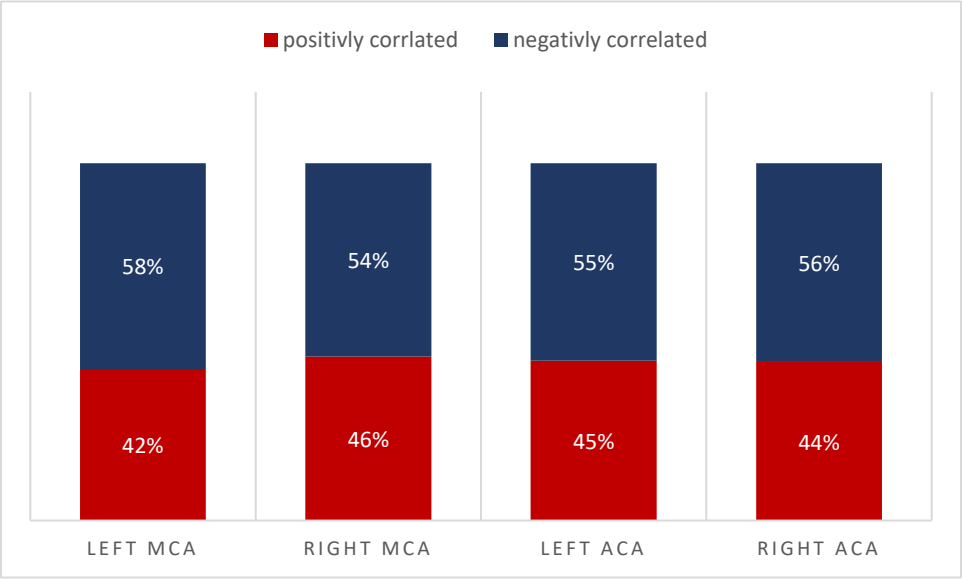

Figure 27. Gray matter voxels correlation to arteries diameter

The VB correlation maps histogram reveals the absolute values of the notable correlated parts are more than 0.3. Thus, if we disregard week correlated regions (in the range of -0.3 to 0.3), the share of negatively correlated voxels in the gray matter gets even more.

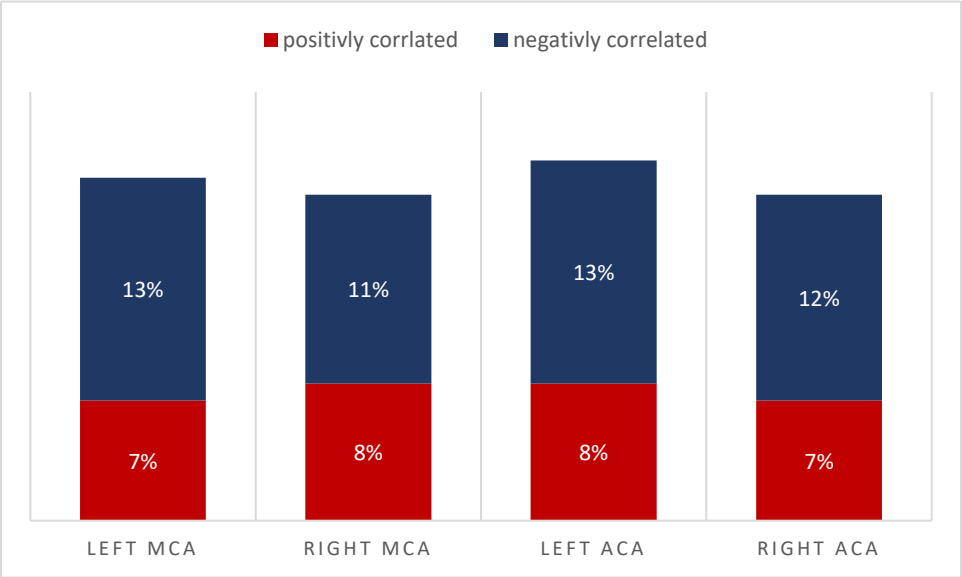

Figure 28. Gray matter voxels correlation to arteries diameter in notable correlated regions

Areas with positive or negative correlations can be detected by in-depth investigation. We used MNI 152 labeled image to detect regions on the correlation map which is also in MNI space. Table 2 illustrates the strongest correlated regions and each artery's diameter with the maximum/minimum r-value.

Table 2. Most correlated regions with arteries' diameter

	Positive correlation	**Negative correlation**
Left middle cerebral artery	Cerebellum Gray Matter (0.65) Left hand Precentral (0.8) Left hand Superior Parietal (0.66)	Medial and Lateral Orbitofrontal cortex (-0.61) Lateral Ventricle (-0.58)
Right middle cerebral artery	Right hand Superior Frontal (0.8)	Right hand Medial Orbitofrontal (-0.56)
Left anterior cerebral artery	Right hand Hippocampus (0.65)	Right hand Cerebellum Gray Matter (-0.67)
Right anterior cerebral artery	Right hand Lateral Ventricle (0.4)	Left hand Entorhinal (-0.61) Left hand Lateral Orbitofrontal (-0.5)

As an example, the left middle cerebral artery's diameter correlation map shows that there is a negative correlation in the Medial and Lateral Orbitofrontal region.

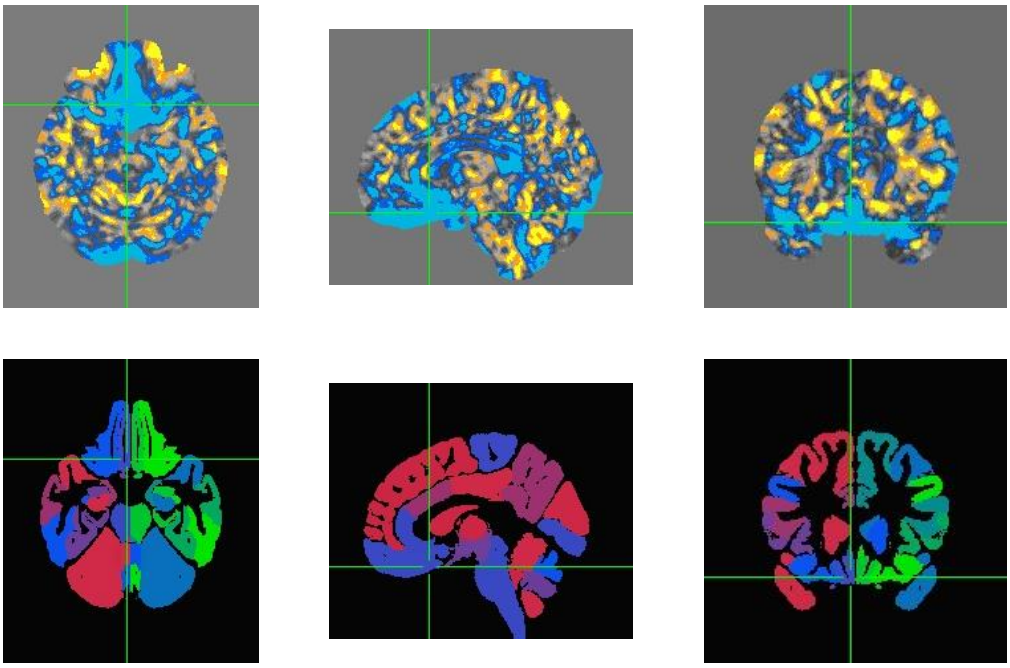

Figure 29. correlation map for left middle cerebral artery (focused on negative value in Medial and Lateral Orbitofrontal cortex)

4.2.2 Surface-based correlation between cortical features extracted by FreeSurfer and arteries diameter

We used FreeSurfer to compute four features (area, thickness, mean curve, volume) for each cortical region of the subjects. In this section, the correlation between cortical features extracted by FreeSurfer and arteries diameter is determined. Here are the matrices showing each region's correlation with each artery's diameter for the four extracted features.

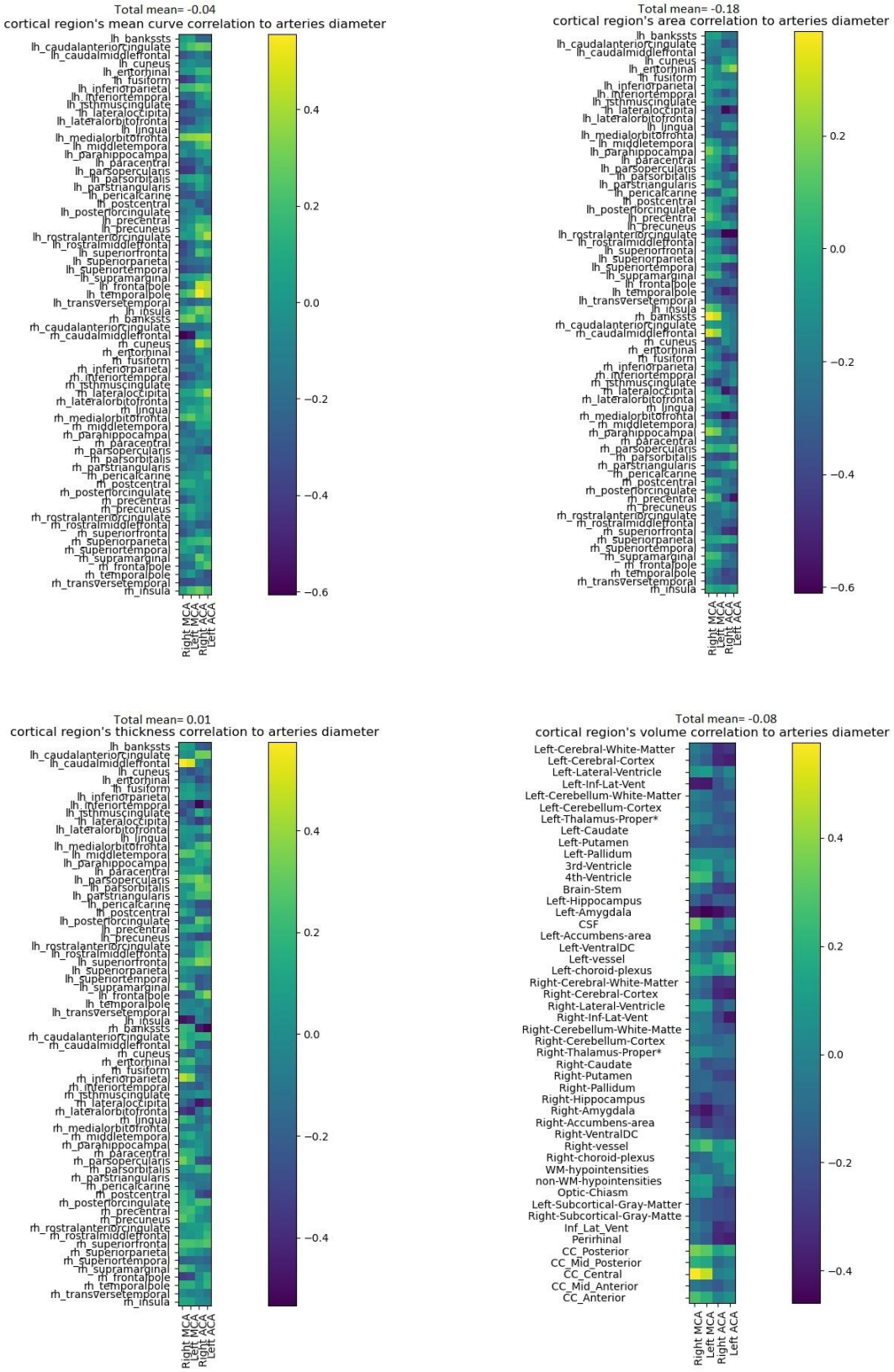

Figure 30. Correlation matrices for extracted features by FreeSurfer and arteries diameter

The strongest correlated regions with each artery's diameter are reported in Table 3.

Table 3. Most correlated regions' features with arteries diameter

	Mean curve	area	thickness	volume
Left middle cerebral artery	Left-hand Medial orbitofrontal (0.36) Right-hand Caudal middle frontal (-0.55)	Right-hand isthmus cingulate (-0.45)	Left-hand caudal middle frontal (0.52) Left-hand insula (-0.44)	Corpus callosum central (0.48) Left & Right Amygdala (-0.46)
Right middle cerebral artery	Left-hand Medial orbitofrontal (0.32) Right-hand Caudal middle frontal (-0.6)	Right-hand isthmus cingulate (-0.35)	Left-hand caudal middle frontal (0.57) Left-hand insula (-0.48)	Corpus callosum central (0.57) Left & Right Amygdala (-0.4)
Left anterior cerebral artery	Left-hand frontal pole (0.43) Right-hand parsopercularis (-0.34)	Left-hand rostral anterior cingulate (-0.6) Right hand precentral (-0.56)	Right hand Lateral occipital (-0.46) Left hand inferior temporal (-0.35)	Left Amygdala (-0.32)
Right anterior cerebral artery	Left-hand temporal pole (0.56) Left-hand postcentral (-0.32)	Left-hand rostral anterior cingulate (-0.61) Left & Right-hand lateral occipital (-0.58)	Right-hand Lateral occipital (-0.39) Left hand inferior temporal (-0.53)	Left Amygdala (-0.42)

Then, we generated 16 maps in which each aparc cortex label was replaced by the r-value of the Spearman correlation coefficient and visualized them on Paraview software.

4.2.2.1 Mean curve correlation maps

According to Figure 31, both middle cerebral arteries diameters are negatively correlated with the right-hand Caudal middle frontal mean curve. Furthermore, the diameter of the anterior cerebral arteries is negatively correlated with the left-hand postcentral mean curve. Meanwhile, the left-hand medial orbitofrontal mean curve is positively correlated with the diameter of those specific arteries. Moreover, the left-hand frontal pole and temporal pole have a positive correlation with anterior cerebral artery diameter.

Left middle cerebral artery

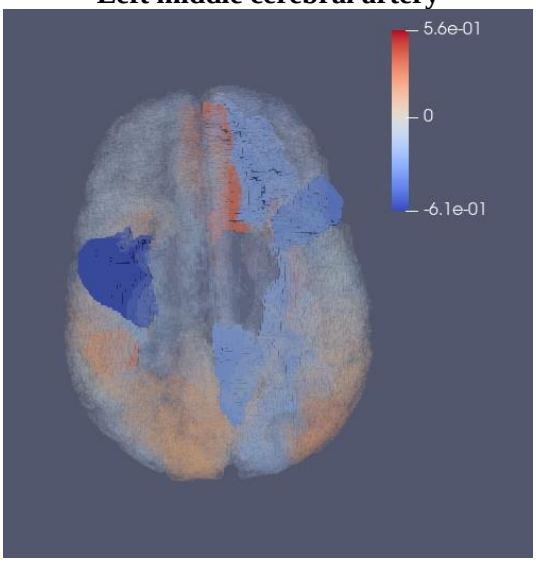

Right middle cerebral artery

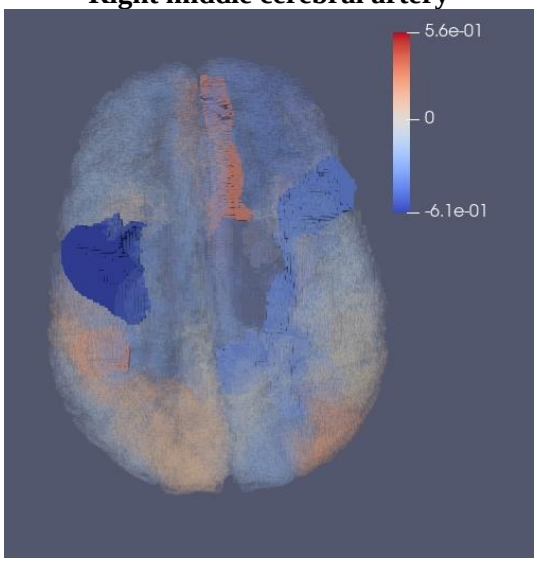

Left anterior cerebral artery

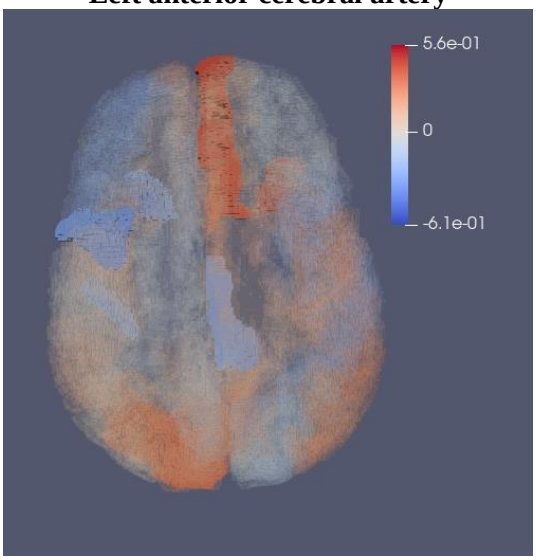

Right anterior cerebral artery

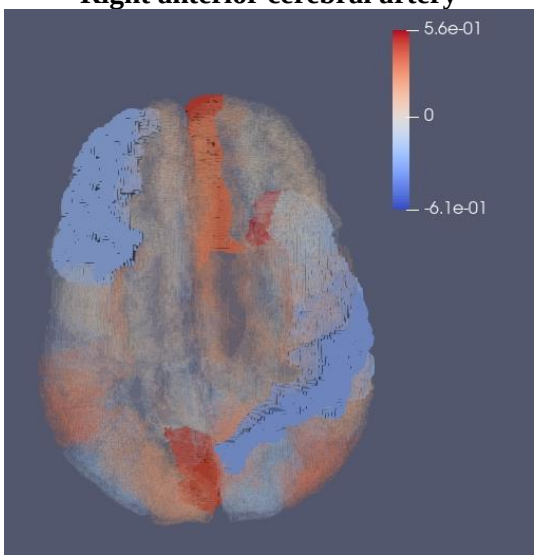

Figure 31. Mean curve correlation with arteries diameter

4.2.2.2 Area correlation maps

Right-hand Caudal middle frontal area has a direct correlation with middle cerebral artery diameter, while its mean curve has an adverse correlation with the same artery. Additionally, the anterior cerebral artery diameter is negatively correlated with the lateral occipital area.

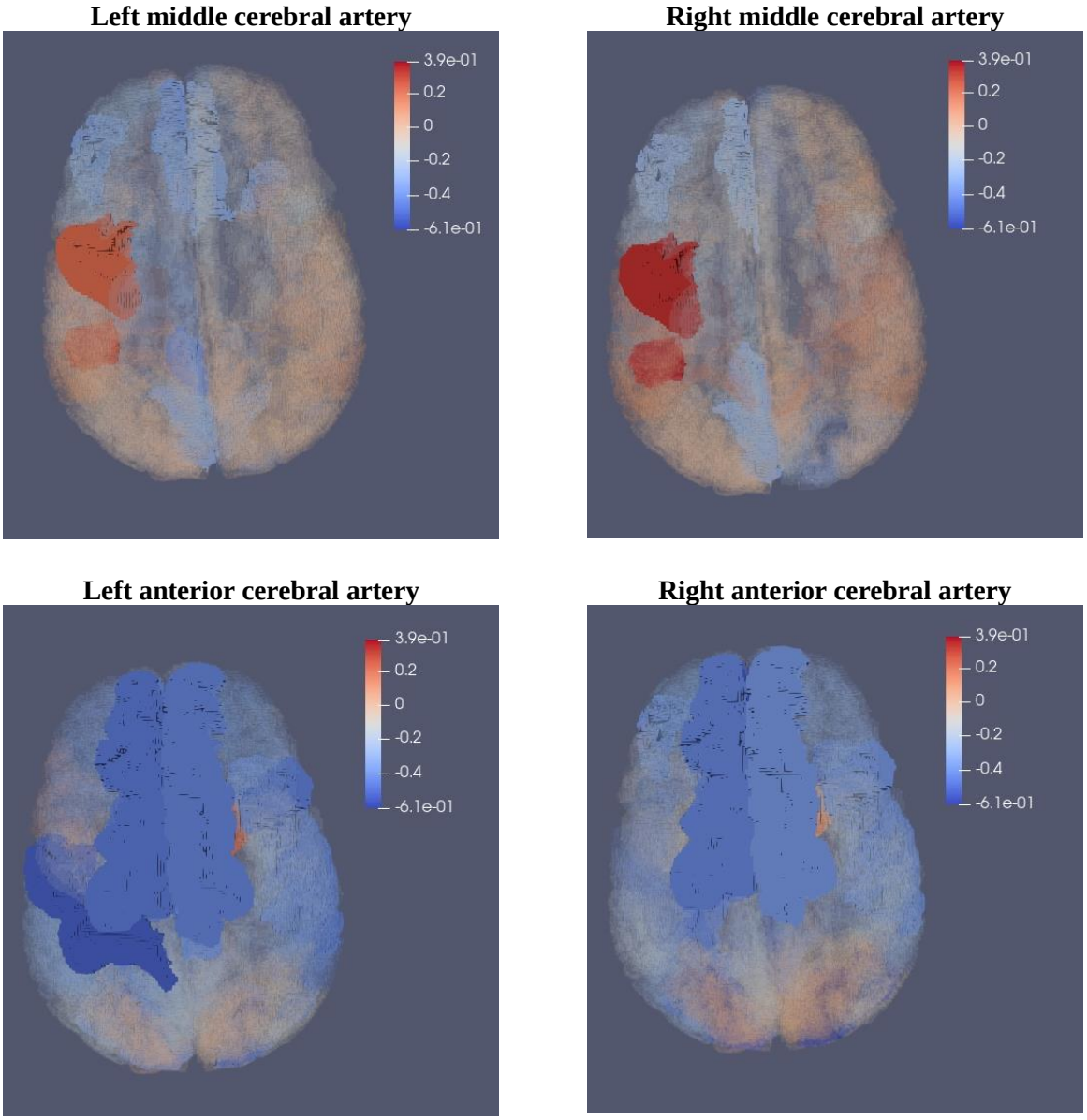

Figure 32. Area correlation with arteries diameter

4.2.2.3 Thickness correlation maps

According to thickness correlation maps, middle cerebral arteries diameter and left-hand caudal middle frontal thickness are positively correlated. A positive correlation exists between anterior cerebral artery diameter and frontal part thickness, but a negative correlation exists between middle and interior region thickness. Right-hand lateral occipital thickness is the most correlated part.

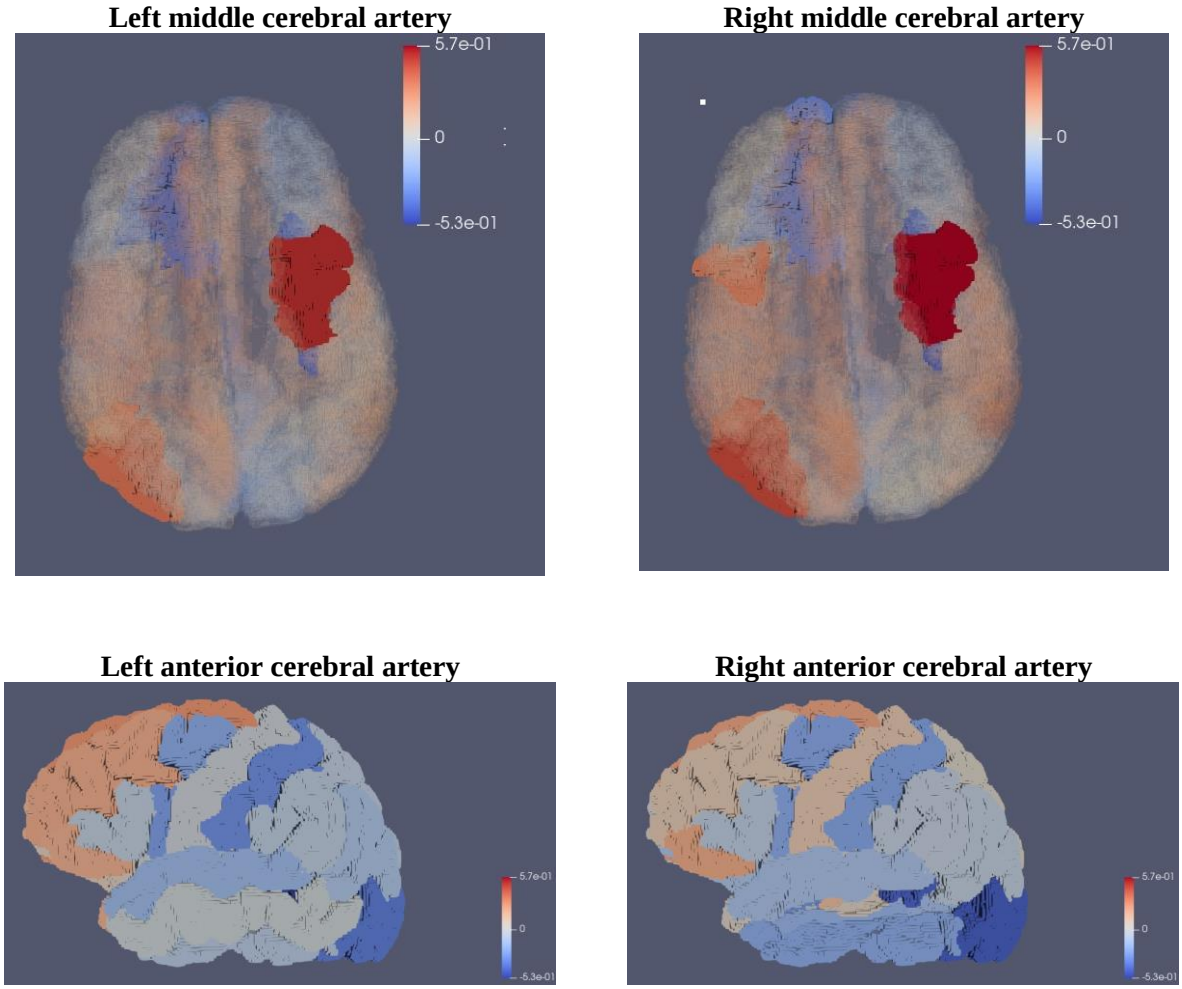

Figure 33. Thickness correlation with arteries diameter

4.2.2.4 Volume correlation maps

Middle artery diameter is less correlated with brain volume. In general, the correlation is negative, with an r-value of around -0.2. Middle cerebral artery diameter and left and right Amygdala volume are the most negatively correlated on a brain map. Ventricle volume and Thalamus volume are lightly correlated with middle artery diameter. The strongest correlation belongs to middle cerebral arteries diameter and central Corpus callosum.

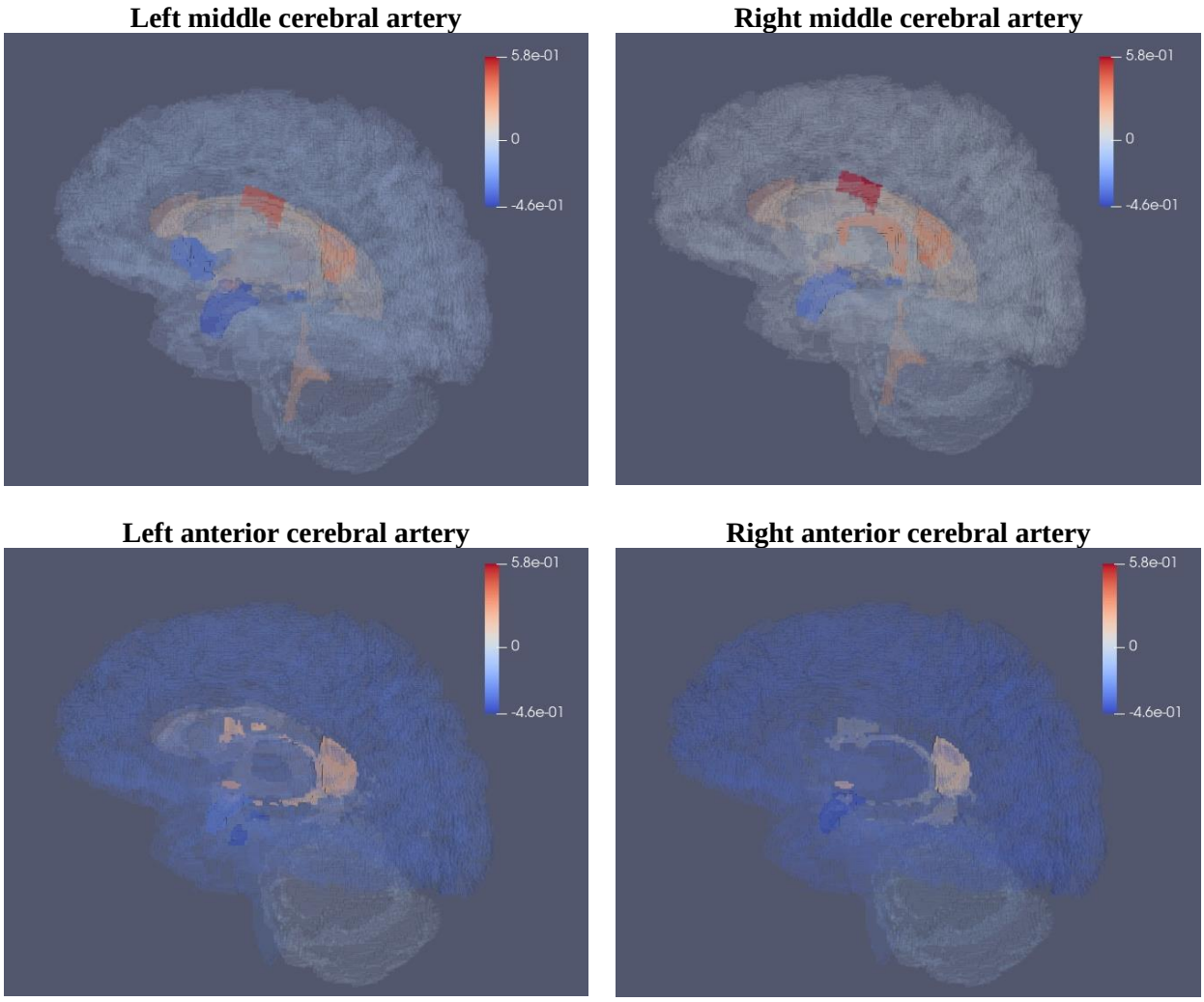

Figure 34. Volume correlation with arteries diameter

4.2.3 Most correlated regions

The mean curvature of the medial orbitofrontal region of the brain has a positive correlation with all four arteries diameter. On the other hand, the region's area didn't show a significant positive correlation, but the lateral occipital area had a negative correlation with the anterior cerebral artery's diameter.

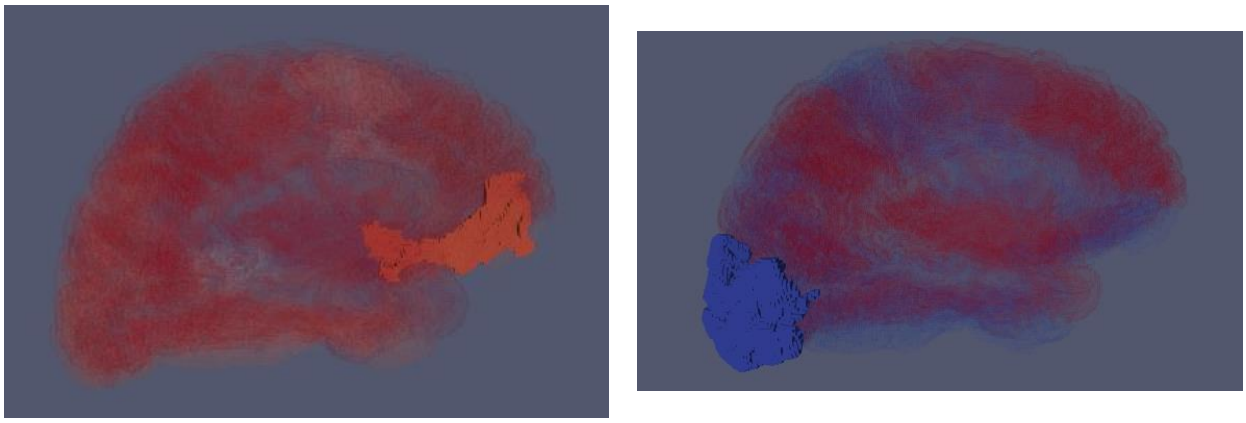

Figure 35. All observed arteries diameter shows a positive correlation with the mean curve and a negative correlation with the area

It is not surprising that anterior cerebral arteries show a positive correlation with anterior region thickness (superior frontal and caudal anterior cingulate) as these arteries supply blood to these regions. The inferior regions' thickness (inferior temporal and lateral occipital) shows a negative correlation with anterior cerebral artery diameter.

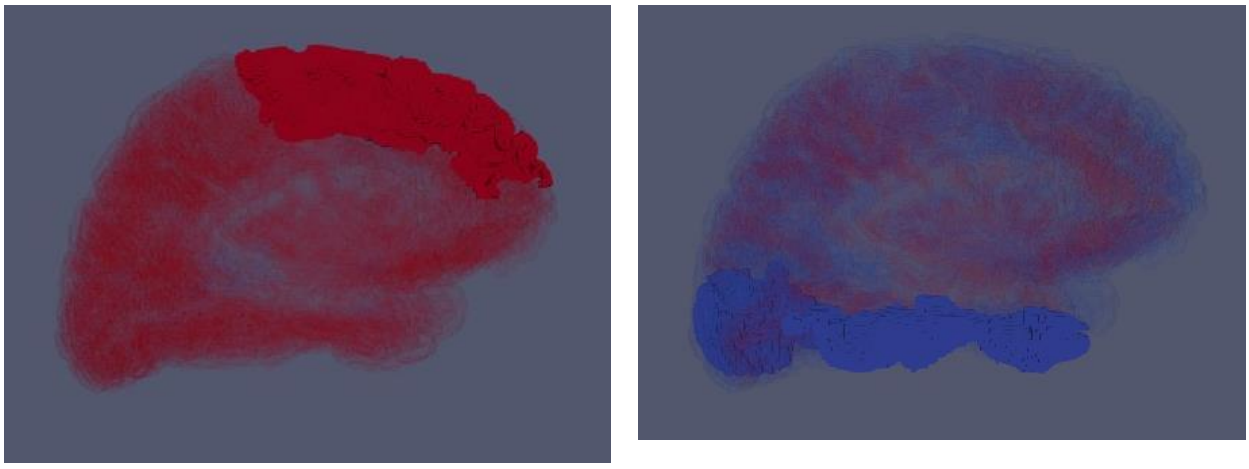

Figure 36. Thickness correlation with anterior cerebral artery’s supplying regions

Amygdala’s decrements do not occur in the same proportion as the overall degree of gray matter loss with aging based on [26]. Our results show foci of significant negative correlation between the Amygdala’s volume and arteries diameter.

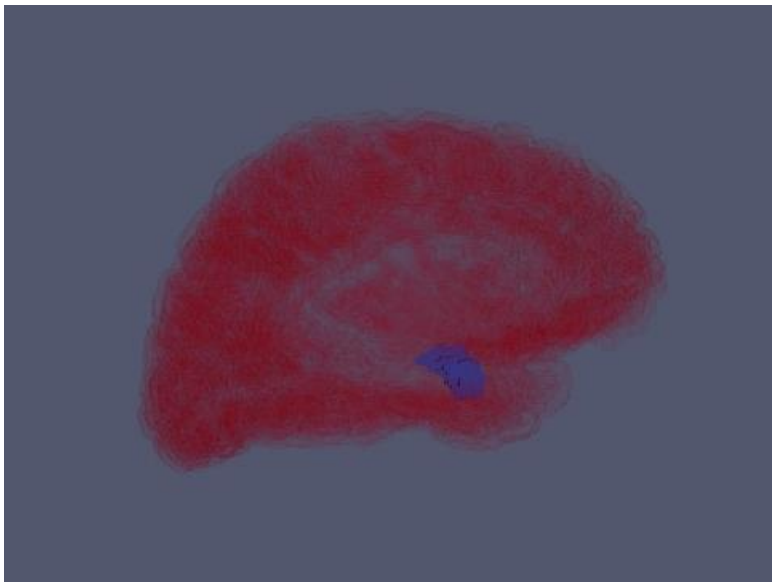

Figure 37. Amygdala’s volume is negatively correlated to arteries diameter

Chapter 5

Conclusion and Future Works

5.1 Conclusion

Based on noninvasive imaging, we provide a processing pipeline to isolate, extract, and quantify cerebral arteries in TOF MRI images and then used the pipeline to investigate if cerebral gray matter metrics could be predicted based on arterial diameter (and vice versa). As a sanity check, we first compared the diameter of the left and right sides of the two types of arteries across subjects. A significant correlation was found between the diameter of the same arteries on opposite sides of the brain, but not between different arteries on the same side of the brain. For example, a subject with large left MCA will also have a large right MCA, but not necessarily a large ACA (on either side). This suggests that there exists some independence across the middle and anterior vascular territories of the brain.

Whole-brain correlation maps were generated using voxel-based and region-based approaches on a popular atlas. Although voxel-based correlation maps show a significant correlation in some regions of gray matter, the mean correlation value of gray matter with each artery's diameter is around 0. The obvious explanation is that the correlation is positive in some regions and negative in others, which lightens the fact that there is almost an equal ratio between gray matter negatively correlated with artery diameter and gray matter positively correlated. VBM shows gray matter inversely correlated with artery diameter, which means larger arteries are associated with less gray matter.

Surface-based correlation maps reveal which feature of each region has a meaningful association with arterial diameter. Overall, we find surface area had the strongest correlation with all arteries, and the relationship was inverse (larger arterial diameter was associated smaller surface area). This finding is counterintuitive as one might expect larger arterial diameters to be correlated to larger surface area (because more cortical tissue requires a larger supply of blood). A positive relationship between the diameter of the anterior cerebral artery and the thickness of the hemisphere supplied by this artery is found, which follows the biological principle that the supply matches the demand.

Our results do not show a significant correlation between cortical volume and artery diameter. This matches the previous research finding that there was no genetic correlation between vascular disease and intracranial volume.

We found a negative correlation between artery diameter and gray matter using both approaches. which means larger arteries are associated with less gray matter.

This conclusion is meaningful based on previous studies I mentioned in the beginning of this presentation. They showed that artery dilatation increases the risk of AD, and people with AD experience a significant reduction of gray matter. We are still investigating possible biophysical explanations for this finding.

5.2 Future work

Despite the numerous tools for the quantification of gray matter and white matter properties in humans, it remains challenging to study the spatial organization and variability of cerebral vessels and assess their impact on brain function. Therefore, the main goal of this study was to create correlation maps of the human cerebrovascular system, which provides a first step toward quantifying morphological changes in the diseased brain and serving as a potential tool in MRI analysis. Further investigation would be needed to arrive at a more complete understanding of the relationship between gray matter and cerebrovascular variability across subjects. Posterior cerebral artery may relate to episodic memory and would show stronger association with gray matter in future works.

References or Bibliography

1. Kirkitadze, M.D., G. Bitan, and D.B. Teplow, Paradigm shifts in Alzheimer's disease and other neurodegenerative disorders: The emerging role of oligomeric assemblies. Journal of Neuroscience Research, 2002. 69(5): p. 567-577.

2. Shoemark, D.K. and S.J. Allen, The Microbiome and Disease: Reviewing the Links between the Oral Microbiome, Aging, and Alzheimer's Disease. Journal of Alzheimer's Disease, 2015. 43: p. 725-738.

3. Baron, J.C., et al., In Vivo Mapping of Gray Matter Loss with Voxel-Based Morphometry in Mild Alzheimer's Disease. NeuroImage, 2001. 14(2): p. 298-309.

4. Dickstein, D.L., et al., Role of Vascular Risk Factors and Vascular Dysfunction in Alzheimer's Disease. Mount Sinai Journal of Medicine: A Journal of Translational and Personalized Medicine, 2010. 77(1): p. 82-102.

5. Gutierrez, J., et al., Brain arterial dilatation and the risk of Alzheimer's disease. Alzheimer's & Dementia, 2019. 15(5): p. 666-674.

6. Agarwal, N. and R.O. Carare, Cerebral Vessels: An Overview of Anatomy, Physiology, and Role in the Drainage of Fluids and Solutes. Frontiers in neurology, 2021. 11: p. 611485-611485.

7. Purves, D. and S.M. Williams, Neuroscience. 2nd edition. 2001: Sinauer Associates 2001.

8. Choi, S., et al., Hemoglobin and mean platelet volume predicts diffuse T1-MRI white matter volume decrease in sickle cell disease patients. NeuroImage: Clinical, 2017. 15.

9. Fundamentals of Magnetic Resonance Imaging, in Breast MRI: Fundamentals and Technical Aspects. 2008, Springer New York: New York, NY. p. 1-17.

10. Brateman, L., The AAPM/RSNA physics tutorial for residents: radiation safety considerations for diagnostic radiology personnel. Radiographics, 1999. 19(4): p. 1037-1055.

11. Pooley, R.A., Fundamental Physics of MR Imaging. RadioGraphics, 2005. 25(4): p. 1087-1099.

12. Mahesh, M., The Essential Physics of Medical Imaging, Third Edition. Med Phys, 2013. 40(7).

13. Ladd, M.E., H.H. Quick, and J.F. Debatin, Interventional MRA and intravascular imaging. J Magn Reson Imaging, 2000. 12(4): p. 534-46.

14. Go with the Flow: MR Angiography, in MRI from Picture to Proton, D.W. McRobbie, et al., Editors. 2017, Cambridge University Press: Cambridge. p. 251-268.

15. Bernier, M., S.C. Cunnane, and K. Whittingstall, The morphology of the human cerebrovascular system. Hum Brain Mapp, 2018. 39(12): p. 4962-4975.

16. Ashburner, J. and K.J. Friston, Voxel-based morphometry--the methods. Neuroimage, 2000. 11(6 Pt 1): p. 805-21.

17. Muhs, B.E., et al., Theory, technique, and practice of magnetic resonance angiography. Vascular, 2007. 15(6): p. 376-83.

18. Bizeau, A., et al., Stimulus-evoked changes in cerebral vessel diameter: A study in healthy humans. J Cereb Blood Flow Metab, 2018. 38(3): p. 528-539.

19. Valdueza, J.M., et al., Changes in blood flow velocity and diameter of the middle cerebral artery during hyperventilation: assessment with MR and transcranial Doppler sonography. AJNR Am J Neuroradiol, 1997. 18(10): p. 1929-34.

20. Joo, B., et al., A deep learning algorithm may automate intracranial aneurysm detection on MR angiography with high diagnostic performance. Eur Radiol, 2020. 30(11): p. 5785-5793.

21. Good, C.D., et al., A Voxel-Based Morphometric Study of Ageing in 465 Normal Adult Human Brains. NeuroImage, 2001. 14(1): p. 21-36.

22. Coffey, C.E., et al., Quantitative cerebral anatomy of the aging human brain: a cross-sectional study using magnetic resonance imaging. Neurology, 1992. 42(3 Pt 1): p. 527-36.

23. Bobinski, M., et al., The histological validation of post mortem magnetic resonance imaging-determined hippocampal volume in Alzheimer's disease. Neuroscience, 2000. 95(3): p. 721-5.

24. Leube, D.T., et al., Neural correlates of verbal episodic memory in patients with MCI and Alzheimer's disease—a VBM study. International Journal of Geriatric Psychiatry, 2008. 23(11): p. 1114-1118.

25. Schmidt-Wilcke, T., et al., Memory performance correlates with gray matter density in the ento-/perirhinal cortex and posterior hippocampus in patients with mild cognitive impairment and healthy controls — A voxel based morphometry study. NeuroImage, 2009. 47(4): p. 1914-1920.

26. Terribilli, D., et al., Age-related gray matter volume changes in the brain during non-elderly adulthood. Neurobiology of Aging, 2011. 32(2): p. 354-368.

27. Zhang, F., et al., Voxel-Based Morphometry: Improving the Diagnosis of Alzheimer's Disease Based on an Extreme Learning Machine Method from the ADNI cohort. Neuroscience, 2019. 414: p. 273-279.

28. Fischl, B., et al., Whole brain segmentation: automated labeling of neuroanatomical structures in the human brain. Neuron, 2002. 33(3): p. 341-55.

29. Fujishima, M., et al., Mild cognitive impairment, poor episodic memory, and late-life depression are associated with cerebral cortical thinning and increased white matter hyperintensities. Front Aging Neurosci, 2014. 6: p. 306.

30. Hutton, C., et al., A comparison between voxel-based cortical thickness and voxel-based morphometry in normal aging. Neuroimage, 2009. 48(2): p. 371-80.

31. ; Available from: https://afni.nimh.nih.gov/.

32. Poldrack, R., et al., Towards open sharing of task-based fMRI data: The OpenfMRI project. Frontiers in neuroinformatics, 2013. 7: p. 12.

33. Smith, S.M., Fast robust automated brain extraction. Human Brain Mapping, 2002. 17(3): p. 143-155.

34. Sarvaiya, J., S. Patnaik, and K. Kothari, Image Registration Using Log Polar Transform and Phase Correlation to Recover Higher Scale. Journal of Pattern Recognition Research, 2012. 7: p. 90-105.

35. Fischl, B., FreeSurfer. NeuroImage, 2012. 62(2): p. 774-781.